

# Optical Jamming Enhances the Secrecy Performance of the Generalized Space Shift Keying Aided Visible Light Downlink

Fasong Wang, Chaowen Liu, Qi Wang, Jiankang Zhang, Rong Zhang, *Senior Member, IEEE*, Lie-Liang Yang, *Fellow, IEEE*, and Lajos Hanzo, *Fellow, IEEE*

## Abstract

In order to enhance the secrecy performance of the Generalized Space Shift Keying (GSSK) visible light communication (VLC) system, in this paper, an optical jamming aided secrecy enhancement scheme is proposed, in which the source transmitter (S) simultaneously sends both the confidential desired signal and optical jamming signals under amplitude and power constraints. The optical jamming signals obey the truncated Gaussian distribution for satisfying the constraints. Given the discrete set of channel inputs, the optical jamming aided GSSK-VLC system's secrecy performance is analyzed. Explicitly, the average mutual information (AMI), the lower bound of AMI and its closed-form approximation as well as the achievable secrecy rate are formulated analytically. Furthermore, the optimal power sharing strategy of the proposed GSSK-VLC systems relying on optical jamming is derived. Finally, closed-form expressions are provided for the optimal power sharing in both the low- and high-SNR regions. Finally, extensive simulation results are presented to validate our analytical results and the secrecy versus bit error ratio (BER) trade-off is characterized.

F. Wang is with the School of Information Engineering, Zhengzhou University, Zhengzhou, 450001, Henan, China. (E-mail: iefswang@zzu.edu.cn)

C. Liu is with the Ministry of Education Key Laboratory for Intelligent Networks and Network Security, Xi'an Jiaotong University, Xi'an, 710049, Shaanxi, China. (E-mail: liucwhb@gmail.com)

Q. Wang, J. Zhang, R. Zhang, L.-L. Yang and L. Hanzo are with Southampton Wireless, School of Electronics and Computer Science, University of Southampton, Southampton SO17 1BJ, UK. (E-mail: qw1e16@soton.ac.uk; z09v@ecs.soton.ac.uk; rz@ecs.soton.ac.uk; lly@ecs.soton.ac.uk; lh@ecs.soton.ac.uk, <http://www-mobile.ecs.soton.ac.uk>)

F. Wang would like to acknowledge the financial support of the NSFC under Grant 61401401, the China Postdoctoral Science Foundation Project under Grant 2015T80779 and the young teachers special Research Foundation Project of Zhengzhou University under Grant 1521318001. L. Hanzo would like to acknowledge the financial support of the ERC's Advanced Fellow Grant Beam-Me-Up.

## Index Terms

Visible light communication (VLC), generalized space shift keying (GSSK), physical layer security (PLS), optical jamming, achievable secrecy rate, power sharing.

## I. INTRODUCTION

In the face of the limited radio-frequency (RF) spectrum [1], visible light communication (VLC) relying on light-emitting diodes (LEDs) both for illumination and for data communications [2] has gained considerable attention from both academia and industry [2]–[4]. However, given the broadcast nature of the VLC downlink, they are inherently vulnerable to eavesdroppers, which are located in the illumination area of the transmitter LEDs. Therefore, similar to their RF counterparts, information privacy and confidentiality to the legitimate VLC users is an important issue, particularly when the communicating nodes are deployed in public areas, such as train stations, offices, shopping malls, etc. [5]. Additionally, securing VLC transmissions is also necessary owing to floor-to-door gaps, keyholes and partially covered windows as well as due to non-line-of-sight (LoS) reflections inside a room [6], [7].

Traditionally, most cryptographic encryption and decryption methods are part of the upper layers of wireless systems [8]. However, these classic encryption techniques may be decrypted in the face of the ever-increasing computational power [9]. As a complement to the conventional upper-layer solutions, such as cryptographic techniques, various physical layer secrecy (PLS) techniques have been proposed to provide perfect security in wireless communication systems [10]–[13], which were first studied in the context of wiretap channels by Wyner in [14] for point-to-point communication systems and later for broadcast channels by Csiszár and Körner in [15], and for Gaussian wiretap channels in [16]. These contributions focused on maximizing the data rate of secret communications, namely, the secrecy capacity of a wiretap channel where a source transmitter (S) is equipped with multiple antennas for confidentially communicating with a legitimate destination receiver (D), while a passive eavesdropper (E) is trying to wiretap the confidential information of S and D. PLS techniques have been applied to a wide range of RF wireless systems, which has improved the overall security by complementing existing classic cryptography-based techniques [11]. However, given the average optical power, the peak optical power and the electrical power constraints imposed on the VLC signals, these techniques developed for RF wireless communication systems

cannot be directly transplanted into practical VLC scenarios. Thus particular designs have to be proposed to avoid new vulnerabilities.

At the time of writing, most of the PLS aided VLC treatises considered single-input single-output (SISO) and multiple-input single-output (MISO) Gaussian wiretap channels. In a little more detail, the upper and lower capacity bounds of the modulation and direct detection (IM/DD) aided SISO VLC channel was investigated in [17]–[19]. As an extension, Chaaban *et.al.* [20] developed the upper and lower bounds for the multiple-input multiple-output (MIMO) channel capacity under the idealized simplifying assumption of having perfect channel state information (CSI) at the transmitter. As one of the key techniques of achieving secrecy, the multi-LED based wiretap channel enjoyed particular attention [5], [21]–[24], where the associated high degree of freedom may be exploited by beamforming schemes [5], [23], [24] and artificial noise injection [21], [22], [25]. Specifically, the authors of [5] derived the lower and upper bounds on the capacity of the SISO Gaussian wiretap channel under continuous input distribution and amplitude constraints. Additionally, when the eavesdropper's channel was exactly known by S, the closed-form secrecy rate expressions were obtained for both MMSE and zero-forcing beamforming strategies. Then, robust secrecy-enhancing beamformers were designed for the secrecy rate maximization of a MISO VLC system, when either the CSI or the CSI-statistics of the eavesdropper was assumed to be perfectly known or imperfectly known [23], [24]. Alternatively, when considering MISO VLC systems, and when the eavesdropper's instantaneous CSI was not available at the transmitter, a friendly jammer was relied upon for transmitting jamming signals by a beamformer to maximize the secrecy rate [21], [22]. Furthermore, to enhance the communication secrecy, a scheme that jointly relies on both transmit beamforming and friendly jamming was proposed for a MISO VLC system operating in the face of multiple eavesdroppers [26].

A common assumption of these contributions is that the distributions of both the channel's input signals and of the jamming signals are continuous. In [5], [23] and [24], a continuous uniform distribution across a given interval was considered, while in [22] and [27] a truncated Gaussian distribution or its generalized form was assumed, where the design-objective was to increase the secrecy rate under a specific amplitude constraint of the input signal. However, the Gaussian input signal assumption is impractical due to its infinite peak power and excessive detection complexity. Additionally, it was found for RF communication that for the SISO Gaussian wiretap channel having both amplitude and power constraints, the channel's input distributions capable of achieving the secrecy capacity rely on finite support sets [28].

However, for the MISO Gaussian wiretap channel, subject to an amplitude constraint, the optimal input signal distributions capable of approaching the secrecy capacity are unknown. For the friendly jammer aided secrecy strategy of classic RF schemes it has been proven that the secrecy rate of any discrete channel inputs associated with finite alphabets is a non-concave function with respect to (w.r.t.) the total transmit power [29]. However, the associated secrecy rate of Gaussian channel inputs is concave and the optimal power allocation has a closed-form expression [30]. Another common feature of the above-mentioned contributions on artificial noise based friendly jamming is that the power sharing between the confidential desired signal and jamming signals has not as yet been considered in the literature, even though it is a critical issue.

The generalized space shift keying (GSSK) modulation technique [31]–[34] is eminently suited for the utilization of multiple LEDs relying on IM/DD techniques in VLC systems. As a result, GSSK aided VLC systems have been extensively studied. However, to the best of our knowledge, there are no achievable secrecy rate performance results in the literature for GSSK-VLC systems. Hence we propose a friendly jammer aided secrecy enhancement scheme and conceive the optimal power sharing between the desired confidential signals and jamming signals.

Explicitly, we consider the PLS issues of GSSK-VLC systems and improve their secrecy performance enhancement with the aid of friendly optical jamming. The contributions of this paper can be summarized as follows.

- A GSSK-VLC system communicating over a Gaussian wiretap channel is conceived, where S transmits its modulated signal jointly with optical jamming signals generated in the null space of the desired channel. The proposed secrecy enhancement scheme does not impose any change on the signals received by the destination, but the eavesdropper will suffer from the intentional optical jamming, regardless of its position. We adopt the truncated Gaussian distribution for the optical jamming signals to satisfy the amplitude constraint.
- The secrecy performance of the GSSK-VLC system relying on optical jamming is analyzed, which includes both the average mutual information (AMI), as well as the lower bound of AMI and its closed-form approximation and finally, the achievable secrecy rate. Additionally, closed-form approximations of the AMI of the Source-to-Destination (S-D) and the Source-to-Eavesdropper (S-E) links are derived, respectively. Furthermore, the influence of the optical jamming signal's amplitude constraint is dis-

cussed, which involves the derivation of the probability density function (PDF) of the sum of independent identical truncated Gaussian distributions, where an approximation is proposed to obtain a closed-form expression.

- The optimal power sharing between the confidential information and the jamming is determined for the sake of maximizing the achievable secrecy rate of the system under amplitude and power constraints. It is indeed plausible that by degrading the performance of E by jamming improves the secrecy, but naturally, the reduced power assigned to the desired link degrades its BER. Specifically, the closed-form expressions of the optimal power sharing factors and the corresponding achievable secrecy rates are derived in both the low- and high signal-to-noise ratio (SNR) regions. Numerical results are presented to show that the proposed optical jamming schemes considerably improve the achievable secrecy rate. Furthermore, we propose a power sharing factor selection technique for striking a trade-off between the secrecy and BER performance according.

The remainder of this paper is organized as follows. The system and channel models are described in Section II. In Section III, our secrecy enhancement relying on optical jamming is proposed and the corresponding secrecy performance is analyzed. Then, in Section IV, the optimal power sharing is derived. Our simulation results and discussions are provided in Section V. Finally, we conclude in Section VI.

*Notation:* Vectors (matrices) are denoted by boldface lowercase (uppercase) letters. The set of  $N$ -dimensional real-valued (non-negative) numbers is denoted by  $\mathcal{R}^N(\mathcal{R}_+^N)$ .  $|\cdot|$ ,  $\|\cdot\|$ ,  $(\cdot)^T$ ,  $[\cdot]$ ,  $\odot$ ,  $\mathbb{E}\{\cdot\}$ ,  $\mathbb{I}(\cdot;\cdot)$ ,  $\binom{\cdot}{\cdot}$  denote absolute value, Euclidean norm, transposition, floor operation, Hadamard product, expected value, mutual information, and binomial coefficient, respectively. We use  $\mathbf{I}_N$  and  $\mathbf{1}$  to denote the  $N$ -dimensional identity matrix and the all-one column vector of length  $N$ , respectively. The curled inequality symbol  $\preceq$  between two vectors denotes componentwise inequality. Superscript  $[x]^+$  denotes  $\max\{x, 0\}$ . A lowercase letter  $x, y, z$  denotes one realization of the random variable  $X, Y, Z$ , respectively. We use the subscripts  $(\cdot)_D$  and  $(\cdot)_E$  to denote relevance to destination (D) and eavesdropper (E), respectively.

## II. SYSTEM DESCRIPTION AND CHANNEL MODELS

In this paper, we assume that the S is installed on the ceiling has  $N_t$  down-facing LEDs and communicates privately with D, which has a single up-facing photo-detector (PD). There is an eavesdropper E, who is also equipped with a single PD<sub>E</sub>. For simplicity, the PD<sub>E</sub> is also

assumed to be facing vertically upwards. The parameters of all LEDs and PDs are assumed to be identical in this paper.

Therefore, the system considered represents a typical multiple-input single-output single-E (MISOSE) VLC Gaussian wiretap channel model. The signals received by D and E are expressed, respectively, as

$$y = \mathbf{h}_D^T \mathbf{x} + w_D, \quad (1)$$

$$z = \mathbf{h}_E^T \mathbf{x} + w_E, \quad (2)$$

where, by definition, we have  $\mathbf{h}_D = [h_{D,1}, h_{D,2}, \dots, h_{D,N_t}]^T \in \mathcal{R}_+^{N_t}$  and  $\mathbf{h}_E = [h_{E,1}, h_{E,2}, \dots, h_{E,N_t}]^T \in \mathcal{R}_+^{N_t}$ , which represent the channel gains of the S-D link and S-E link, respectively. We assume that S exploits the full knowledge of  $\mathbf{h}_D$  but no knowledge about  $\mathbf{h}_E$ . We assume that E can estimate its own channel gains  $\mathbf{h}_E$ . In (1) and (2),  $\mathbf{x} = [x_1, x_2, \dots, x_{N_t}]^T \in \mathcal{R}^{N_t}$  is an information-bearing signal vector sent by S, which is assumed to be a zero-mean signal vector superimposed on an identical direct current (DC) bias  $I_{DC} \in \mathcal{R}_+$  for adjusting the illumination level of LEDs [5]. For safety reason and to avoid clipping distortion, we assume that the total current  $I_{DC} + x_{n_t}$  is restricted within the range of  $(I_{DC} - \alpha I_{DC}, I_{DC} + \alpha I_{DC})$ , where  $\alpha \in [0, 1]$  is termed as the modulation index [5], [17]. In other words,  $\mathbf{x}$  is subject to the amplitude constraint termed as  $|\mathbf{x}| \preceq A\mathbb{1}$ , where  $A = \alpha I_{DC}$ . Finally, in (1) and (2),  $w_D \sim \mathcal{N}(0, \sigma_D^2)$  and  $w_E \sim \mathcal{N}(0, \sigma_E^2)$  are zero-mean additive white Gaussian noise (AWGN) processes, received by D and E, respectively.

When the LEDs are installed on the ceiling facing down, the channel model may neglect all non-LoS components, hence we only consider the LoS signal component for obtaining tractable analytical results [5], [23], [24], [35]. Then, assuming a generalized Lambertian emission pattern, the path gain  $G_{D,n_t}$  between the  $n_t$ -th LED and the PD<sub>D</sub> can be represented as [5], [36],

$$G_{D,n_t} = \begin{cases} \frac{1}{2\pi d_{n_t}^2} (\check{m} + 1) A_{R_x} \cos^{\check{m}}(\phi) \cos \psi_{n_t}, & |\psi_{n_t}| \leq \Psi_{\text{FoV}}, \\ 0, & |\psi_{n_t}| > \Psi_{\text{FoV}}, \end{cases} \quad (3)$$

where  $d_{n_t}$  is the LoS distance between the  $n_t$ -th LED and the PD<sub>D</sub>,  $\phi$  is the angle of irradiance of the LED,  $\psi_{n_t}$  is the angle of incidence of the  $n_t$ -th optical link, which is measured from the axis perpendicular to the receiver surface,  $\check{m} = -1/\log_2(\cos \Phi_{1/2})$  is the order of Lambertian emission with half irradiance at semi-angle  $\Phi_{1/2}$ , which is measured from the optical axis of the LED, and  $\Psi_{\text{FoV}}$  is the receiver's field-of-view (FoV) semi-angle. Finally,  $A_{R_x}$  is the

effective detection area of the PD, which is given by [36]

$$A_{\text{Rx}} = \frac{\beta^2}{\sin^2(\Psi_{\text{FoV}})} A_{\text{PD}}, \quad (4)$$

where  $\beta$  is the refractive index of the optical concentrator and  $A_{\text{PD}}$  is the PD area. Then, the VLC channel gain between the  $n_t$ -th LED and the  $\text{PD}_D$  can be expressed as  $h_{D,n_t} = TRG_{D,n_t}\eta$ ,  $n_t = 1, 2, \dots, N_t$ , where  $T$  is the gain of a transimpedance amplifier,  $R$  is the responsivity of the PD and  $\eta$  is the current-to-light conversion efficiency of the LEDs, respectively. Similarly, the channel gain between the  $n_t$ -th LED and the  $\text{PD}_E$  can be expressed as  $h_{E,n_t} = TRG_{E,n_t}\eta$ , for  $n_t = 1, 2, \dots, N_t$ .

Note that the channel gain of a VLC link depends on the specific position of the transmitter LED and the receiver PD. If a receiver PD is not in a transmitter's FoV, the channel gain of the link will be zero [5].

### III. OPTICAL JAMMING AIDED GSSK-VLC SYSTEM AND ITS PERFORMANCE ANALYSIS

In this section, the performance of the GSSK-VLC system relying on optical jamming is considered. Firstly, the GSSK-VLC system and signal model are introduced. Then, the optical jamming aided GSSK-VLC scheme is designed for improving the secrecy performance. Finally, the secrecy performance of the optical jamming aided GSSK-VLC system is analyzed.

#### A. GSSK-VLC System and Signals Modelling

We assume that there are  $N$  LEDs in the room considered, among which a subset of  $N_t$  LEDs are utilized for communication. Specifically, we assume that  $N_t$  out of  $N$  LEDs are employed for GSSK modulation. Then, during a specific symbol period,  $n_t$  ( $1 \leq n_t < N_t$ ) LEDs are activated to transmit an information symbol, while the remaining  $(N_t - n_t)$  LEDs are only used for illumination. Hence, there are in total  $M' = \binom{N_t}{n_t}$  possible combinations, among which  $M = 2^m$  with  $m = \lfloor \log_2 M' \rfloor$  are used transmitting  $m$  bits per symbol. In our ensuring analysis, we explicitly assume that the first  $M$  combinations are used for conveying the information.

Let a GSSK symbols be expressed as  $x \in \mathcal{X}$ , where  $\mathcal{X}$  is the set of  $M$  possible GSSK symbols. Based on  $x$ ,  $n_t$  out of  $N_t$  LEDs are activated to transmit, with each having a constant intensity of  $I = s/\sqrt{n_t}$ , where the factor of  $1/\sqrt{n_t}$  is used for attaining the total power constraint. Correspondingly, the transmitted signal vector  $\mathbf{x}$  can be expressed as

$$\mathbf{x} = \frac{s}{\sqrt{n_t}} \sum_{n_i=1}^{n_t} \mathbf{e}_{\omega_{n_i}} = \frac{s}{\sqrt{n_t}} \underbrace{[1 \ \dots \ 0 \ 1 \ 0 \ \dots \ 1 \ \dots \ 0]}_{n_t \text{ out of } N_t \text{ non-zero elements}}^T = \frac{s}{\sqrt{n_t}} \mathbf{e}_{\omega}, \quad (5)$$

where  $\mathbf{e}_{\omega_{n_i}}$ ,  $\omega_{n_i} \in \{1, 2, \dots, N_t\}$ , represents a specific column of an identity matrix  $\mathbf{I}_{N_t}$ , with the  $\omega_{n_i}$ -th element being one. Hence,  $\mathbf{e}_\omega = \sum_{n_i=1}^{n_t} \mathbf{e}_{\omega_{n_i}}$  is a  $N_t$ -length vector with  $n_t$  non-zero elements corresponding to the  $n_t$  activated LEDs, and  $\omega \in \Omega = \{1, 2, \dots, M\}$ . Without loss of generality, we assume that the average intensity of  $\mathbf{x}$  is normalized, so that we have  $\mathbb{E}\{\|\mathbf{x}\|^2\} = 1$ , implying that  $s^2 = 1$ .

Note that, the GSSK-VLC system is reduced to a space shift keying (SSK) VLC system, when  $n_t = 1$ . Therefore, the SSK-VLC scheme is a special case of our GSSK-VLC. Hence, all the following analysis can be applied to SSK-VLC by letting  $n_t = 1$ .

When the signal of (5) is transmitted over the VLC wiretap channel, following (1) and (2), we have

$$y = \mathbf{h}_D^T \mathbf{x} + w_D = \frac{s}{\sqrt{n_t}} \mathbf{h}_D^T \mathbf{e}_\omega + w_D = h_{D(\omega)} s + w_D, \quad (6)$$

$$z = \mathbf{h}_E^T \mathbf{x} + w_E = \frac{s}{\sqrt{n_t}} \mathbf{h}_E^T \mathbf{e}_\omega + w_E = h_{E(\omega)} s + w_E, \quad (7)$$

where by definition, we have  $h_{D(\omega)} = \frac{\mathbf{h}_D^T \mathbf{e}_\omega}{\sqrt{n_t}} \in \mathcal{H}_{D(\omega)}$  and  $h_{E(\omega)} = \frac{\mathbf{h}_E^T \mathbf{e}_\omega}{\sqrt{n_t}} \in \mathcal{H}_{E(\omega)}$ , with  $\mathcal{H}_{D(\omega)}$  and  $\mathcal{H}_{E(\omega)}$  being the two sets collecting all the  $M$  possible channel states observed at D and E, respectively, when S transmits one of the  $M$  legitimate symbols.

### B. Optical Jamming Aided GSSK-VLC System

In this subsection, we enhance the secrecy performance of the S-D link by the optical jamming of E's reception, hence degrading its signal-to-interference-plus-noise ratio (SINR). In a practical GSSK-VLC system, it is reasonable to assume that S does not have the CSI of the S-E link for a passive eavesdropper. However, S may transmit an optical jamming signal along with the modulated GSSK signal in the nullspace of the S-D channel. In principle, whilst S transmits a symbol using a set of  $n_t$  approximately selected LEDs, all the  $N_t$  LEDs can additionally be utilized to emit jamming signals without degrading the reception of D. In this case, D is capable of receiving its information as in the conventional GSSK system, while E experiences intentional interference. Consequently, the secrecy performance can be enhanced without degrading the reception of D. However, the secrecy performance enhancement is achieved at the cost of activating more LEDs and by assigning additional power to the jamming signals, whilst maintaining the same total power.

The system model of the GSSK-VLC system relying on optical jamming is illustrated in Fig. 1. With the aid of the classic singular value decomposition (SVD) [37], we can express



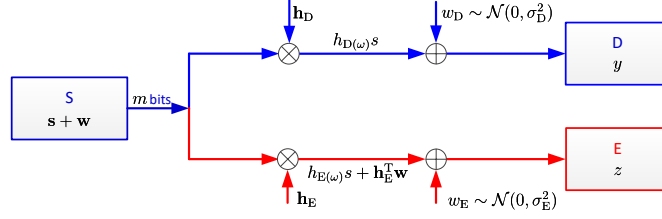


Fig. 1. System model of the GSSK-VLC Gaussian wiretap channel relying on optical jamming.

$\mathbf{h}_D$  as

$$\mathbf{h}_D^T = [\lambda, \mathbf{0}^T][\mathbf{v}_s, \mathbf{V}_n]^T, \quad (8)$$

where  $\lambda$  is the singular value. From (8), we obtain a null space  $\mathbf{V}_n = [\mathbf{v}_1, \mathbf{v}_2, \dots, \mathbf{v}_{N_t-1}] \in \mathcal{R}^{N_t \times (N_t-1)}$ , since  $\mathbf{h}_D$  has  $\text{rank}(\mathbf{h}_D) = 1$ . Then, the optical jamming signals emitted by S can be designed to obey

$$\mathbf{w} = \mathbf{V}_n \mathbf{u}, \quad (9)$$

where  $\mathbf{u} = [u_1, u_2, \dots, u_{N_t-1}]^T \in \mathcal{R}^{N_t-1}$  is a time-varying jamming signal vector, whose entries are from a real-valued truncated Gaussian distribution [38] confined to the interval of  $[-\frac{A}{N_t-1}, \frac{A}{N_t-1}]$ .

For a real-valued random variable defined as  $\tilde{P} \sim \mathcal{N}(\mu, \sigma^2)$ , we denote the double-sided truncated Gaussian random variable of  $\tilde{P}$  as  $P$ , whose PDF is expressed as  $\mathcal{TN}(\mu, \sigma^2, -B, B)$ , and is given by

$$f_P(p) = \frac{\frac{1}{\sqrt{2\pi\sigma^2}} \exp\left(-\frac{(p-\mu)^2}{2\sigma^2}\right)}{\Phi\left(\frac{B-\mu}{\sigma}\right) - \Phi\left(\frac{-B-\mu}{\sigma}\right)} I_{[-B, B]}(p), \quad (10)$$

where  $\Phi(\cdot)$  is the Gaussian cumulative distribution function (CDF),  $I_{[-B, B]}(p)$  is the indicator function satisfying  $I_{[-B, B]}(p) = 1$  if  $p \in [-B, B]$  and  $I_{[-B, B]}(p) = 0$ , otherwise. In our scheme, we set  $u_{n_i} \sim \mathcal{TN}(0, \frac{\sigma_j^2}{N_t-1}, -\frac{A}{N_t-1}, \frac{A}{N_t-1})$ ,  $n_i = 1, 2, \dots, N_t - 1$ , as seen in Fig. 1.

Upon involving the jamming signals, the signals transmitted from the  $N_t$  LEDs of the system can now be expressed as

$$\mathbf{x} = \mathbf{s} + \mathbf{w} = \frac{s}{\sqrt{n_t}} \mathbf{e}_\omega + \mathbf{V}_n \mathbf{u}. \quad (11)$$

In the proposed GSSK-VLC system, the total transmit power is constrained by

$$\mathbb{E}\{\|\mathbf{x}\|^2\} = \mathbb{E}\{\mathbf{x}^T \mathbf{x}\} = \mathbb{E}\{\mathbf{s}^T \mathbf{s} + \mathbf{w}^T \mathbf{w}\} = s^2 + \sigma_j^2 = 1. \quad (12)$$

Hence, the optimal power can be assigned to the desired signals and to jamming by appropriately adjusting  $s^2$  and  $\sigma_j^2$  in (12). Consequently, the observations attained by D and E can be respectively expressed as

$$y = \mathbf{h}_D^T \mathbf{x} + w_D = \frac{s}{\sqrt{n_t}} \mathbf{h}_D^T \mathbf{e}_\omega + \mathbf{h}_D^T \mathbf{w} + w_D = h_{D(\omega)} s + w_D, \quad (13)$$

$$z = \mathbf{h}_E^T \mathbf{x} + w_E = \frac{s}{\sqrt{n_t}} \mathbf{h}_E^T \mathbf{e}_\omega + \mathbf{h}_E^T \mathbf{w} + w_E = h_{E(\omega)} s + \mathbf{h}_E^T \mathbf{V}_n \mathbf{u} + w_E, \quad (14)$$

where (13) is valid, because  $\mathbf{h}_D$  is orthogonal to  $\mathbf{w}$ . As (13) and (14) indicate, the secrecy performance of D and E is the same in the GSSK-VLC system considered, if no optical jamming is imposed on E's reception. However, when jamming is provided by  $\mathbf{w}$ , D's reception is not affected, while E's reception may be severely degraded, hence resulting in an improved secrecy performance for D.

### C. Secrecy Performance of Optical Jamming Aided GSSK-VLC System

In the following, we derive the AMI between S and E. Based on the results obtained, we can then evaluate the AMI between S and D by letting  $\mathbf{w} = \mathbf{0}$ . Let  $\check{w}_E$  denote the equivalent noise observed by E. Then, from (14), we have

$$\check{w}_E = \mathbf{h}_E^T \mathbf{w} + w_E = \mathbf{h}_E^T \mathbf{V}_n \mathbf{u} + w_E = \sum_{i=1}^{N_t-1} u_i \mathbf{h}_E^T \mathbf{v}_i + w_E, \quad (15)$$

which is the sum of  $N_t$  independent identically distributed (i.i.d.) variables. Since the resultant aggregate distribution is given by the convolution of this set of double-sided truncated Gaussian variables, the distribution of  $\check{w}_E$  is difficult to derive in a closed form. Even for the sum of two variables obeying the double-sided truncated Gaussian distribution, the resultant PDF becomes complicated. Specifically, let  $X_1 \sim \mathcal{TN}(\mu_{x_1}, \sigma_{x_1}, a_{x_1}, b_{x_1})$ ,  $X_2 \sim \mathcal{TN}(\mu_{x_2}, \sigma_{x_2}, a_{x_2}, b_{x_2})$  and  $f(x_i, \mu, \sigma) = \frac{1}{\sqrt{2\pi}\sigma} e^{-\frac{(x_i - \mu)^2}{2\sigma^2}}$ , as well as denote  $Z_1 = X_1 + X_2$ . Then, the PDF of  $Z_1$  is in the form of

$$f_{Z_1}(z_1) = \frac{\int_{\delta_1}^{\delta_2} f_1 f_2 dx_1}{\Phi_1 \Phi_2}, \quad (16)$$

where  $\delta_1 = \max\{a_{x_1}, z_1 - b_{x_2}\}$ ,  $\delta_2 = \min\{b_{x_1}, z_1 - a_{x_2}\}$ ,  $f_1 = f(x_1, \mu_{x_1}, \sigma_{x_1})$ ,  $f_2 = f(z_1 - x_1, \mu_{x_2}, \sigma_{x_2})$ ,  $\Phi_1 = \Phi(b_{x_1}, \mu_{x_1}, \sigma_{x_1}) - \Phi(a_{x_1}, \mu_{x_1}, \sigma_{x_1})$ ,  $\Phi_2 = \Phi(b_{x_2}, \mu_{x_2}, \sigma_{x_2}) - \Phi(a_{x_2}, \mu_{x_2}, \sigma_{x_2})$ . Furthermore, for deriving the PDF of  $\check{w}_E$ , we have to compute the convolution of  $f_{Z_1}(z_1)$  and the PDF of a Gaussian distributed  $w_E$ , which is excessively complex. Hence we invoke the central limit theorem, which states that the sum of  $n$  i.i.d. signals tends to the Gaussian

distribution, as  $n$  becomes large. In practice, the number of transmit LEDs is sufficiently high, hence we can be confident that  $\check{w}_E$  has a near-Gaussian distribution.

It can be shown that the mean of  $\check{w}_E$  is zero, while its covariance obeys

$$\begin{aligned}\Omega_E &= \mathbb{E}\{\check{w}_E\check{w}_E^T\} = \mathbb{E}\left\{\left(\sum_{n_i=1}^{N_t-1} u_{n_i}\mathbf{h}_E^T\mathbf{v}_{n_i} + w_E\right)\left(\sum_{n_j=1}^{N_t-1} u_{n_j}\mathbf{h}_E^T\mathbf{v}_{n_j} + w_E\right)^T\right\} \\ &\stackrel{(a)}{=} \mathbb{E}\left\{\left(\mathbf{h}_E^T\sum_{n_i=1}^{N_t-1} u_{n_i}\mathbf{v}_{n_i}\right)\left(\mathbf{h}_E^T\sum_{n_j=1}^{N_t-1} u_{n_j}\mathbf{v}_{n_j}\right)^T\right\} + \sigma_E^2 \\ &= \frac{\sigma_J^2}{N_t-1}\mathbf{h}_E^T\left(\sum_{n_i=1}^{N_t-1}\mathbf{v}_{n_i}\mathbf{v}_{n_i}^T\right)\mathbf{h}_E + \sigma_E^2 = \frac{\sigma_J^2}{N_t-1}\mathbf{h}_E^T\mathbf{V}_n\mathbf{V}_n^T\mathbf{h}_E + \sigma_E^2,\end{aligned}\quad (17)$$

where equality (a) holds, because  $\{u_{n_i}\}_{n_i=1}^{N_t-1}$  and  $w_E$  are statistically independent. Consequently, the received signal of E can be expressed with the aid of the Gaussian approximation as

$$z = h_{E(\omega)}s + \check{w}_E. \quad (18)$$

Furthermore, after normalizing  $z$  by multiplying it with  $\Omega_E^{-1/2}$ , we arrive at:

$$\tilde{z} = \Omega_E^{-1/2}h_{E(\omega)}s + \Omega_E^{-1/2}\check{w}_E = \tilde{h}_{E(\omega)}s + \tilde{w}_E, \quad (19)$$

where  $\tilde{w}_E$  has a zero mean and unit variance, and, by definition,  $\tilde{h}_{E(\omega)} = \Omega_E^{-1/2}h_{E(\omega)}$ . Consequently, the conditional and unconditional PDFs of E's received signal  $\tilde{z}$  can be expressed as

$$f_{\tilde{z}|\tilde{h}_E}(\tilde{z}|\tilde{h} = \tilde{h}_{E(\omega)}) = \frac{1}{\sqrt{2\pi}}\exp\left(-\frac{(\tilde{z} - \tilde{h}_{E(\omega)}s)^2}{2}\right), \quad (20)$$

$$f_{\tilde{z}}(\tilde{z}) = \sum_{\omega \in \Omega} \frac{1}{\sqrt{2\pi}M} \exp\left(-\frac{(\tilde{z} - \tilde{h}_{E(\omega)}s)^2}{2}\right), \quad (21)$$

respectively. Similarly, the conditional and unconditional PDFs of  $y$  can be respectively expressed as

$$f_{Y|h_D}(y|h = h_{D(\omega)}) = \frac{1}{\sqrt{2\pi}\sigma_D} \exp\left(-\frac{(y - h_{D(\omega)}s)^2}{2\sigma_D^2}\right), \quad (22)$$

$$p_Y(y) = \sum_{\omega \in \Omega} p_{Y|h_D}(y|h_{D(\omega)})P_{h_D}(h_{D(\omega)}) = \sum_{\omega \in \Omega} \frac{1}{\sqrt{2\pi}\sigma_D M} \exp\left(-\frac{(y - h_{D(\omega)}s)^2}{2\sigma_D^2}\right). \quad (23)$$

According to [39], the AMI between two probability spaces remains invariant to a reversible transformation, implying that the transformation of (19) does not change the AMI.

Consequently, given the PDF expressions of (20)-(23), the AMIs of both the S-D link and of the S-E link can be obtained, which are stated in Theorem 1.

*Theorem 1:* For the GSSK-VLC system relying on both optical jamming and on finite discrete inputs, the AMI of the S-D channel is

$$\mathbb{I}^J(h_D; Y) = \log_2 M - \frac{1}{M} \sum_{\omega=1}^M \mathbb{E}_{w_D} \left[ \log_2 \sum_{\varpi=1}^M \exp \left( \frac{1}{2} \varrho_D (w_D^2 - (w_D + \zeta_{\omega, \varpi} s)^2) \right) \right], \quad (24)$$

where  $\zeta_{\omega, \varpi} = h_{D(\omega)} - h_{D(\varpi)}$ , and the AMI of S-E channel is

$$\mathbb{I}^J(h_E; Z) = \log_2 M - \frac{1}{M} \sum_{\omega=1}^M \mathbb{E}_{\tilde{w}_E} \left[ \log_2 \sum_{\varpi=1}^M \exp \left( \frac{1}{2} \left( \tilde{w}_E^2 - (\tilde{w}_E + \Omega_E^{-1/2} \xi_{\omega, \varpi} s)^2 \right) \right) \right], \quad (25)$$

where  $\xi_{\omega, \varpi} = h_{E(\omega)} - h_{E(\varpi)}$ .

*Proof:* Please refer to Appendix A. ■

Given  $\mathbb{I}^J(h_D; Y)$  and  $\mathbb{I}^J(h_E; Z)$ , as shown in (24) and (25), the secrecy rate achievable by D can be expressed as  $R_{\text{sec}}^J = [\mathbb{I}^J(h_D; Y) - \mathbb{I}^J(h_E; Z)]^+$ .

In order to simplify the results of (24) and (25), the lower bounds for the AMI of the S-D and S-E links can be derived, which are given by the following theorem.

*Theorem 2:* The AMI of the S-D channel can be lower bounded by

$$\mathbb{I}_L^J(h_D; Y) = \log_2 M - \frac{1}{2} (\log_2 e - 1) - \frac{1}{M} \sum_{\omega=1}^M \log_2 \sum_{\varpi=1}^M \exp \left( -\frac{(\zeta_{\omega, \varpi} s)^2}{4\sigma_D^2} \right). \quad (26)$$

The AMI of the S-E channel can be lower-bounded by

$$\mathbb{I}_L^J(h_E; Z) = \log_2 M - \frac{1}{2} (\log_2 e - 1) - \frac{1}{M} \sum_{\omega=1}^M \log_2 \sum_{\varpi=1}^M \exp \left( -\frac{(\xi_{\omega, \varpi} s)^2}{4\Omega_E} \right). \quad (27)$$

*Proof:* Please refer to Appendix B. ■

Furthermore, based on Theorem 1 and Theorem 2, below we derive the approximate expressions for  $\mathbb{I}^J(h_D; Y)$  and  $\mathbb{I}^J(h_E; Z)$ , respectively. Firstly, when  $\varrho_D \rightarrow \infty$  and  $\varrho_D \rightarrow 0$ , we can derive the limits of (24)  $\mathbb{I}^J(h_D; Y)$ , which are

$$\lim_{\varrho_D \rightarrow \infty} \mathbb{I}^J(h_D; Y) = \log_2 M \quad \text{and} \quad \lim_{\varrho_D \rightarrow 0} \mathbb{I}^J(h_D; Y) = 0. \quad (28)$$

Secondly, we can obtain the limits of  $\mathbb{I}_L^J(h_D; Y)$  from (26) for  $\varrho_D \rightarrow \infty$  and  $\varrho_D \rightarrow 0$  as

$$\lim_{\varrho_D \rightarrow \infty} \mathbb{I}_L^J(h_D; Y) = \log_2 M - \frac{1}{2} (\log_2 e - 1) \quad \text{and} \quad \lim_{\varrho_D \rightarrow 0} \mathbb{I}_L^J(h_D; Y) = -\frac{1}{2} (\log_2 e - 1). \quad (29)$$

When we compare the results in (28) and (29), we can see that there is a constant gap of  $\frac{1}{2} (\log_2 e - 1)$  between the AMI and its corresponding lower bound in both the high- and low-SNR regions. Furthermore, it can be shown that both  $\mathbb{I}^J(h_D; Y)$  and  $\mathbb{I}_L^J(h_D; Y)$  are

monotonically increasing functions w.r.t.  $\rho_D$ . It can be readily inferred from these observations that for any given SNR, especially for an SNR located in the high- or low-SNR region, the difference between  $\mathbb{I}^J(h_D; Y)$  and  $\mathbb{I}_L^J(h_D; Y)$  should approximately be a constant of  $\frac{1}{2}(\log_2 e - 1)$ . Based on similar arguments, we can also quantify the difference between  $\mathbb{I}^J(h_E; Z)$  and  $\mathbb{I}_L^J(h_E; Z)$ , which is also approximately a constant of  $\frac{1}{2}(\log_2 e - 1)$ .

Therefore, we may conclude that  $\mathbb{I}^J(h_D; Y)$  can be closely approximated as  $\mathbb{I}^J(h_D; Y) \approx \mathbb{I}_L^J(h_D; Y) + \frac{1}{2}(\log_2 e - 1)$ , and from Theorem 2, we have

$$\mathbb{I}_S^J(h_D; Y) \approx \log_2 M - \frac{1}{M} \sum_{\omega=1}^M \log_2 \sum_{\varpi=1}^M \exp \left( -\frac{(\zeta_{\omega, \varpi} s)^2}{4\sigma_D^2} \right). \quad (30)$$

Similarly, we have

$$\mathbb{I}_S^J(h_E; Z) \approx \log_2 M - \frac{1}{M} \sum_{\omega=1}^M \log_2 \sum_{\varpi=1}^M \exp \left( -\frac{(\xi_{\omega, \varpi} s)^2}{4\Omega_E} \right). \quad (31)$$

Consequently, by subtracting (31) from (30), the approximate secrecy rate of D in our GSSK-VLC system relying on optical jamming can be expressed as

$$\begin{aligned} R_{S, \text{sec}}^J &= [\mathbb{I}_S^J(h_D; Y) - \mathbb{I}_S^J(h_E; Z)]^+ = \left[ \frac{1}{M} \sum_{\omega=1}^M \log_2 \left[ \frac{\sum_{\varpi=1}^M \exp \left( -\frac{(\xi_{\omega, \varpi} s)^2}{4\Omega_E} \right)}{\sum_{\varpi=1}^M \exp \left( -\frac{(\zeta_{\omega, \varpi} s)^2}{4\sigma_D^2} \right)} \right] \right]^+, \\ &= \frac{1}{M} (\Upsilon_2 - \Upsilon_1), \end{aligned} \quad (32)$$

where, by definition,

$$\Upsilon_1 = \sum_{\omega=1}^M \log_2 \sum_{\varpi=1}^M \exp \left( -\frac{(\zeta_{\omega, \varpi} s)^2}{4\sigma_D^2} \right), \quad (33)$$

and

$$\Upsilon_2 = \sum_{\omega=1}^M \log_2 \sum_{\varpi=1}^M \exp \left( -\frac{(\xi_{\omega, \varpi} s)^2}{4\Omega_E} \right). \quad (34)$$

#### IV. OPTIMAL POWER SHARING

In order to achieve the highest secrecy rate possible for the proposed optical jamming aided GSSK-VLC system, there is an optimal power sharing between the information-bearing signal and jamming signals. Let the total power per transmission be denoted by  $\mathcal{P}$ . As described in Section II, we have  $\mathcal{P} = s^2 + (N_t - 1)\sigma_u^2 = s^2 + \sigma_j^2$ . Without loss of generality, we assume that  $\sigma_D^2 = \sigma_E^2 = \sigma^2 = 1/\rho$ . Then, if the portion of power allocated to the information-bearing signal is denoted as

$$s^2 = \kappa \mathcal{P}, \quad (35)$$

the associated jamming power becomes:

$$\sigma_J^2 = (1 - \kappa)\mathcal{P}. \quad (36)$$

In the proposed GSSK-VLC system, we assume that the channel  $h_{D(\omega)}$  is known to S. Hence, according to  $h_{D(\omega)}$ , S can adapt the value of  $\kappa$  to achieve the optimal secrecy rate, which is hence referred to as the adaptive power sharing. Specifically, with the aid of the approximate closed-form expressions of (32) derived for the secrecy rate, the optimal value of  $\kappa$  set for achieving the highest secrecy rate at different SNRs can be found by a one-dimensional search, albeit at the cost of a relatively high complexity. Hence, below we analyze the behavior of the optimal value of  $\kappa$ , when the system is operated either in the low- or in the high-SNR region.

For convenience, we define  $d_\omega = \frac{1}{M} \sum_{\varpi=1}^M \zeta_{\omega,\varpi}^2$ , which represents the average value of the squared difference of the channel gain between S and D, when activating  $n_t$  LEDs. Similarly, we define  $g_\omega = \frac{1}{M} \sum_{\varpi=1}^M \xi_{\omega,\varpi}^2$ , representing the average value of the squared difference of the channel gain between S and E, when activating  $n_t$  LEDs. Furthermore, we define  $\bar{d} = \frac{1}{M} \sum_{\omega=1}^M d_\omega = \frac{1}{M^2} \sum_{\omega=1}^M \sum_{\varpi=1}^M \zeta_{\omega,\varpi}^2$  and  $\bar{g} = \frac{1}{M} \sum_{\omega=1}^M g_\omega = \frac{1}{M^2} \sum_{\omega=1}^M \sum_{\varpi=1}^M \xi_{\omega,\varpi}^2$ . Additionally, we define  $\chi = \mathbf{h}_{E,\omega}^T \mathbf{V}_n \mathbf{V}_n^T \mathbf{h}_{E,\omega}$ . With the aid of the above definitions, we first make the following observations.

*Theorem 3:* When the proposed optical jamming aided GSSK-VLC system is operated in the low-SNR region of  $\rho \ll 1$  and when  $\bar{d} > \bar{g}$ , the value of  $\kappa$  maximizing  $R_{S,\text{sec}}^J$  is  $\kappa = 1$ . When  $\rho \ll 1$  and  $\bar{d} < \bar{g}$ , we should maximize the jamming power by letting  $\kappa = 0$ , which results in a secrecy rate  $R_{S,\text{sec}}^J(\kappa)$  of 0.

*Proof:* Please refer to Appendix C. ■

It should be noted that, when  $\bar{d} = \bar{g}$  and when operating in the low-SNR region, we also have  $R_{S,\text{sec}}^J = 0$ . In this case, the spatial distributions of D and E are identical when viewed from S.

From the proof of Theorem 3, we know that  $(1 - \frac{1}{4}\rho\mathcal{P}M\bar{g}\kappa) \geq 0$  and  $(1 - \frac{1}{4}\rho\mathcal{P}M\bar{d}\kappa) \geq 0$  should be satisfied. With the aid of these conditions, we can determine the region of low SNR. Based on our simulations, we found that provided that for  $\text{SNR} \leq 3$  dB, we satisfy the conditions required for Theorem 3.

As for the power-sharing in the high-SNR region, for an arbitrary  $\omega$ , we define  $\zeta_\omega^{\min} = \min_{\varpi \neq \omega, \varpi=1, \dots, M} \{\zeta_{\omega,\varpi}^2\}$ , and denote by  $\ell_\omega$  the total number of this kind of minimum elements. Furthermore, we define  $\zeta^{\min} = \min_{\omega=1, \dots, M} \{\zeta_\omega^{\min}\}$  and denote by  $\ell$  the total number of the

TABLE I  
THE DISTRIBUTIONS OF THE LEDs' LOCATIONS

2 LEDs		8 LEDs	
LED	$(O_X, O_Y, O_Z)$	1	(1.25, 0.625, 3.0) m
1	(1.25, 2.50, 3.0) m	2	(3.75, 0.625, 3.0) m
2	(3.75, 2.50, 3.0) m	3	(1.25, 1.875, 3.0) m
4 LEDs		4	(3.75, 1.875, 3.0) m
1	(1.25, 1.25, 3.0) m	5	(1.25, 3.125, 3.0) m
2	(3.75, 1.25, 3.0) m	6	(3.75, 3.125, 3.0) m
3	(1.25, 3.75, 3.0) m	7	(1.25, 4.375, 3.0) m
4	(3.75, 3.75, 3.0) m	8	(3.75, 4.375, 3.0) m

minimum of  $\zeta^{\min}$ . Then, the optimum power-sharing is given by the following Theorem.

*Theorem 4:* When the proposed optical jamming aided GSSK-VLC system is operated in the high-SNR region of  $\varrho \gg 1$ , the optimal value of  $\kappa$  is

$$\kappa = \frac{4}{\varrho \mathcal{P} \zeta^{\min}} \ln \left( \frac{\varrho \mathcal{P} \zeta^{\min} \chi^\ell}{M \bar{g}} - \ell \right), \quad (37)$$

which yields the maximum secrecy rate  $R_{S,sec}^J$  of

$$R_{S,sec}^J(\kappa) = \log_2 M + \frac{1}{M} \left[ \log_2 \left( 1 - \frac{1}{4\chi} \kappa M \bar{g} \right) - \log_2 \left[ 1 + \ell \exp \left( -\frac{\varrho \kappa \mathcal{P} \zeta^{\min}}{4} \right) \right] \right]. \quad (38)$$

*Proof:* Please refer to Appendix D. ■

## V. SIMULATIONS AND NUMERICAL RESULTS

In this section, to validate the analytical secrecy performance and to demonstrate the efficiency of the proposed optical jamming secrecy enhancement strategy, we provide numerical results for an indoor VLC environment having the dimensions of  $[5 \times 5 \times 3] \text{ m}^3$ , represented by a three-dimensional (3D) Cartesian coordinate system  $[O_X, O_Y, O_Z]$  with the origin being in one corner of the room. Again, the transmit LEDs are assumed to be perpendicular to the ceiling and down-facing to the floor. Similarly, the receivers (D and E) are located on the desks at the height of 0.85 m from the floor, which are assumed to be perpendicular to the desk and facing the ceiling. Unless specially noted, we assume that the positions of LEDs are those presented in Table I.

The half-illuminance semi-angle of LED  $\Phi_{1/2}$  is set to be  $60^\circ$ , which is a typical value for commercially-available high-brightness LEDs [5]. Both D and E have a  $60^\circ$  FoV (semi-angle), the area of each PD is  $A_{PD} = 1.0 \text{ cm}^2$  and the responsivity is  $R = 100 \mu\text{A/mW/cm}^2$

TABLE II  
SIMULATION PARAMETERS

Simulation setup	
Room size ( $L \times W \times H$ )	$5 \times 5 \times 3 \text{ m}^3$
Number of LEDs	2, 4, 8
LEDs (D) height	3 m
Receivers (Bob and Eve) height	0.85 m
Transmitter parameters	
Semi-angle at half power ( $\Phi_{1/2}$ )	$60^\circ$
Optical power/ electric conversion efficiency ( $\eta$ )	$813.6 \mu\text{W}/\text{mA}$
Modulation index ( $\alpha$ )	0.1
Receiver parameters	
Refractive index ( $\beta$ )	1.5
Physical area of a PD ( $A_{\text{PD}}$ )	$1.0 \text{ cm}^2$
Receiver FoV semi-angle ( $\Psi_{\text{FoV}}$ )	$60^\circ$
PD responsivity ( $R$ )	$100 \mu\text{A}/\text{mW}/\text{cm}^2$

[5]. For convenience, all the parameters involved in our simulations are summarized in Table II.

#### A. Secrecy Performance of the Proposed GSSK-VLC Systems

To investigate the secrecy performance of the proposed optical jamming aided secrecy-enhancing scheme, a typical VLC scenario is considered, where we assume that D is located at (2.15, 1.28, 0.85) m. Unless specifically noted, we assume that the power allocated to the information signal and jamming signals is equal, i.e.,  $\kappa = 0.5$ . It should be noted that in practical applications, it is unreasonable to constrain D to a specific location. Actually, in our simulations, the D's location is selected randomly, hence the corresponding results are valid for all the areas that D can reach.

Fig. 2 depicts the AMI between S and E from (25) and its lower bound from (27) for the GSSK-VLC systems operating both with and without optical jamming, where  $N_t = 2, 4, 8$  for SSK-VLC systems and  $N_t = 8, n_t = 2$  for GSSK-VLC system. E is located at (2.60, 0.88, 0.85) m, all other parameters involved in this simulation are taken from Table I and Table II. Observe from the simulation results that upon increasing the SNR, both  $\mathbb{I}(h_E; Z)$  and  $\mathbb{I}_L(h_E; Z)$  tend to constant values. Moreover,  $\mathbb{I}(h_E; Z)$  and  $\mathbb{I}_L(h_E; Z)$  also increase, as the number of LEDs  $N_t$  and that of the activated LEDs  $n_t$  is increased. Furthermore, the



gap between  $\mathbb{I}(h_E; Z)$  and  $\mathbb{I}_L(h_E; Z)$  in the low- and high-SNR regions is approximately a constant of  $\frac{1}{2}(\log_2 e - 1)$ , which coincides with the theoretical analysis. It should be noted that the gap between  $\mathbb{I}(h_E; Z)$  and  $\mathbb{I}_L(h_E; Z)$  in the high-SNR region of all four cases is slightly higher than  $\frac{1}{2}(\log_2 e - 1)$ . This is due to the approximation error of using  $\mathcal{N}(0, 1)$  to estimate the distribution of  $\tilde{w}_E$ . Additionally, Fig. 2 reveals that the proposed optical jamming strategy is capable of dramatically decreasing the AMI between S and E for all the cases considered. In particular, for the GSSK scenario associated with  $N_t = 8, n_t = 2$ , when SNR = 40 dB, the AMI between S and E is  $\mathbb{I}(h_E; Z) = 3.55$  bits/symbol. After applying optical jamming, we have  $\mathbb{I}(h_E; Z) = 1.06$  bits/symbol, which is reduced substantially. Hence, all the proposed GSSK-VLC systems are capable of achieving an improved secrecy performance, when employing the optical jamming advocated.

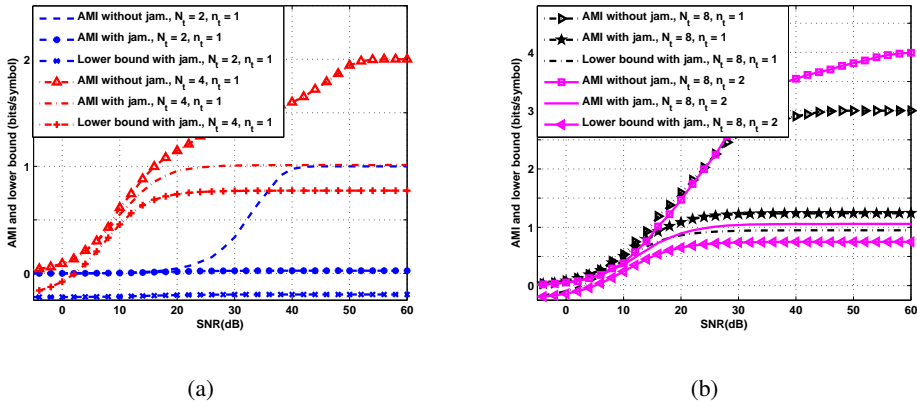


Fig. 2. AMI between S and E as well as its lower bound performance (a)  $N_t = 2, 4, n_t = 1$  in the SSK-VLC and (b)  $N_t = 8, n_t = 1, 2$  in the SSK- and GSSK-VLC systems with and without optical jamming. The results were calculated from (25) and (27).

Fig. 3 characterizes both the AMI and the achievable secrecy rate between S and D from (24) as well as that between S and E from (25) in Section III-C. The achievable secrecy rate of the VLC systems operating with and without optical jamming calculated from (32) is shown, where we have  $N_t = 2, 4, 8$  for our SSK-VLC systems as well as  $N_t = 8, n_t = 2$  for the GSSK-VLC system, and E is located at  $(2.60, 0.88, 0.85)$  m. All other parameters involved in this simulation are taken from Table I and Table II. It is seen that in all the four cases, the achievable secrecy rate increases as the SNR increases, which is the explicit benefit of optical jamming.

Fig. 4 demonstrates the achievable secrecy rate of the SSK-VLC system from (32) with optical jamming, where  $N_t = 4, n_t = 1$ . E's location is varied across the 2D plane at a height of 0.85 m, while D's position is fixed  $(2.15, 1.28, 0.85)$  m, all other parameters involved in

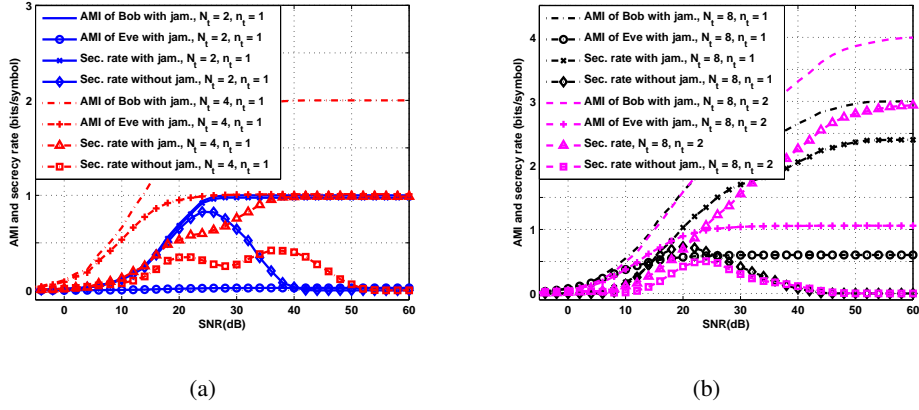


Fig. 3. AMI between S and D as well as that between S and E, and achievable secrecy rate performance (a)  $N_t = 2, 4, n_t = 1$  in the SSK-VLC and (b)  $N_t = 8, n_t = 1, 2$  in the SSK- and GSSK-VLC systems with and without optical jamming. The results were calculated from (24), (25) and (32).

this simulation are taken from Table I and Table II. The SNR is 30 dB. It can be observed from Fig. 4 that in most of the area considered, the SSK-VLC system achieves a relatively stable secrecy rate. However, as shown in [40], the achievable secrecy rate of the SSK-VLC system is zero in most of the scenarios considered, if no secrecy enhancement is utilized. The main reason behind this is that even for high SNRs, the detection performance of E can still be degraded by optical jamming, without affecting the reception performance of D, since the jamming signals are designed to lie in the null space of  $\mathbf{h}_D$ .

To make the above statement more convincing, in Fig. 5, we quantify the achievable secrecy rate of the GSSK-VLC system ( $N_t = 8, n_t = 2$ ) from (32) by letting SNR = 40 dB and by using the same parameters as in the above example. As shown in Fig. 5, the GSSK-VLC system achieves a relatively stable secrecy rate. As expected, when E moves close to D, the achievable secrecy rate is significantly reduced. However, the achievable secrecy rate of the GSSK-VLC system increases rapidly, as E moves away from D. Additionally, when E is located at the symmetric regions of the projection of the transmitters, the achievable secrecy rate increases, which confirms the analytical results of [40].

### B. Optical Power Sharing

Fig. 6 shows the impact of different power sharing factors  $\kappa$  on the achievable secrecy rate of the GSSK-VLC system for low SNRs, the simulation results here are evaluated from Theorem 3, where  $N_t = 8, n_t = 1$ , while D is located at (2.15, 1.28, 0.85) m and E is located at (2.60, 1.88, 0.85) m, all other parameters involved in this simulation are taken from Table I and Table II. In this case, as implied by the theoretical results of Theorem 3, when  $\bar{d} > \bar{g}$ , the proposed GSSK-VLC system should allocate as much power to the information-bearing

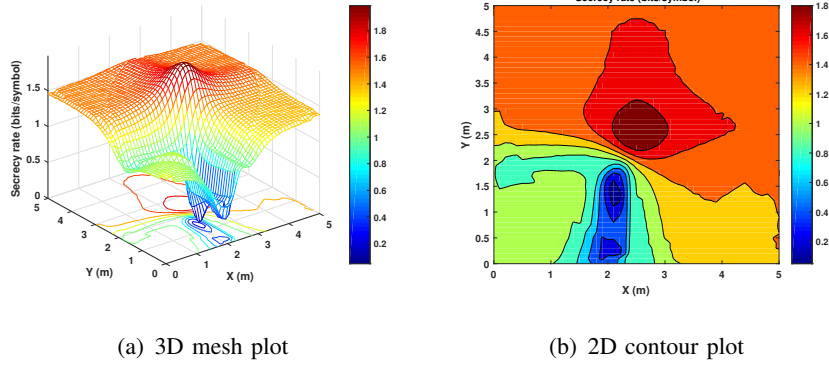


Fig. 4. Secrecy rate achieved by the SSK-VLC system with optical jamming. (a) 3D mesh plot; (b) 2D contour plot. The results were calculated from (32).

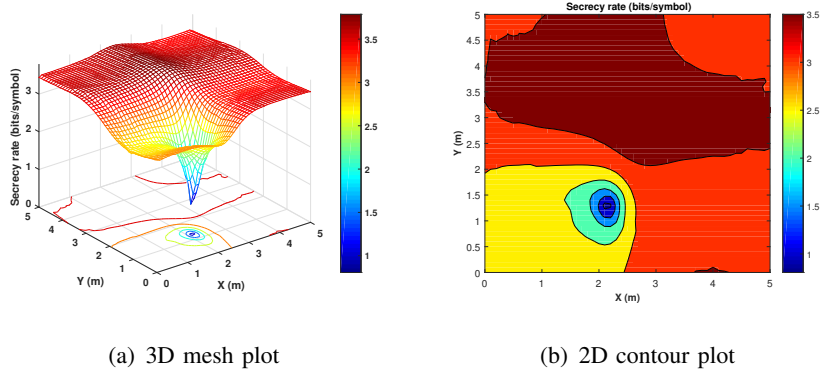


Fig. 5. Secrecy rate achieved by the GSSK-VLC system with optical jamming. (a) 3D mesh plot; (b) 2D contour plot. The results were calculated from (32).

desired signal as possible, so as to achieve enhanced secrecy. Observe from Fig. 6(a) that for the low SNRs investigated, the achievable secrecy rate improves as the power allocated to the information-bearing signal increases, which confirms the analytical results of Section IV. On the other hand, when  $\bar{d} < \bar{g}$ , Fig. 6(b) demonstrates the result of  $\mathbb{I}_S^J(h_D; Y) - \mathbb{I}_S^J(h_E; Z)$  for the GSSK-VLC system having different power sharing factors  $\kappa$  and low SNRs. As expected, in this case, even though an increased fraction of the power should be allocated to the jamming signals to enhance the system's secrecy, the achievable secrecy rate of the proposed GSSK-VLC system still remains zero. However, in practice, in order to avoid this unintended situation, we may adopt the user-centric LED allocation philosophy of [41] for ensuring that D always has better channel conditions than E, i.e.,  $\bar{d} > \bar{g}$ . From the results of Fig. 6(a) and Fig. 6(b), we conclude that in the low-SNR region, the power should be predominantly assigned to the information-bearing signal.

Fig. 7 depicts the optimal power sharing factor and the corresponding achievable secrecy rate obtained from (37) and (38) for our proposed GSSK-VLC systems at high SNRs from Theorem 4 vs. the SNR. Observe that the achievable secrecy rate  $R_{S,sec}^J$  reaches its maximum

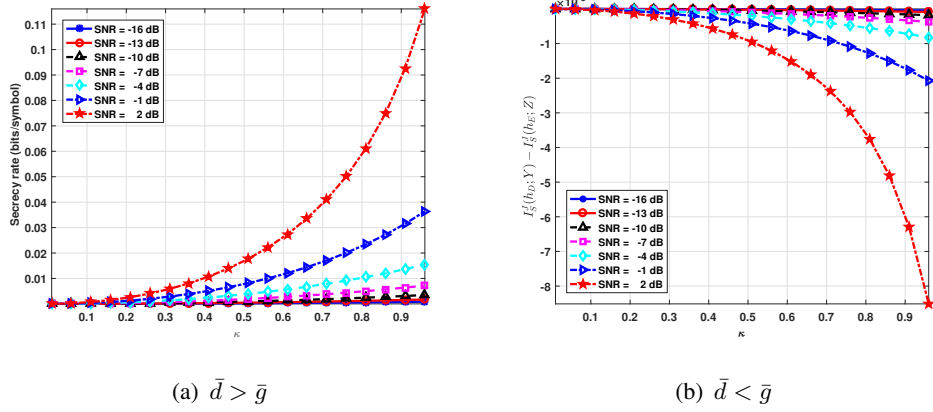


Fig. 6. (a) Achievable secrecy rate of the GSSK-VLC systems vs. the power sharing factor  $\kappa$  at low SNRs, when  $\bar{d} > \bar{g}$ ; (b)  $I_S^J(h_D; Y) - I_S^J(h_E; Z)$  results of the GSSK-VLC systems vs. the power sharing factor  $\kappa$  at low SNRs, where  $\bar{d} < \bar{g}$ . The results were calculated from Theorem 3 and (50).

at the highest SNR and the smallest power sharing factor  $\kappa$  for the investigated four cases, where we have  $N_t = 2, 4, 8$  for the SSK-VLC systems and  $N_t = 8, n_t = 2$  for the GSSK-VLC system, while D is located at (2.15, 1.28, 0.85) m and E is located at (2.60, 1.88, 0.85) m, all other parameters involved in this simulation are taken from Table I and Table II. We can also observe that  $R_{S,sec}^J$  approaches its minimum, when the SNR is relatively low and a small proportion of the power is allocated to transmit jamming in our SSK-VLC system having  $N_t = 2, 4, 8$ . Especially, for our GSSK-VLC system associated with  $N_t = 8, n_t = 2$ ,  $R_{S,sec}^J$  approaches its minimum when  $\kappa = 1$  and when the SNR is relatively low. The reason behind this is that as both  $N_t$  and  $n_t$  increase, the channel's correlation becomes higher, which will reduce the signal intensity received at D when SNR is relatively low. Additionally, in all the above-mentioned four cases,  $R_{S,sec}^J$  reaches its maximum, when the SNR is relatively high and almost more than half of the power is allocated to transmit optical jamming, i.e. we have  $\kappa \leq 0.5$ .

### C. BER vs Secrecy Performance Trade-off of the Proposed GSSK-VLC Systems

Fig. 8 shows the BER performance of E for the GSSK-VLC systems relying on optical jamming and different power sharing factors  $\kappa$ . Observe from the simulation results that the BER performance of E is dramatically degraded due to the optical jamming. We also see that when the portion of power allocated to the jamming signal exceeds a threshold, such as 0.5 in the high-SNR region, the reduction of  $\kappa$  appears to have a negligible impact on the BER performance of E. However, the BER performance of D is heavily degraded when more power is allocated to optical jamming, which can be observed in the Fig. 9.

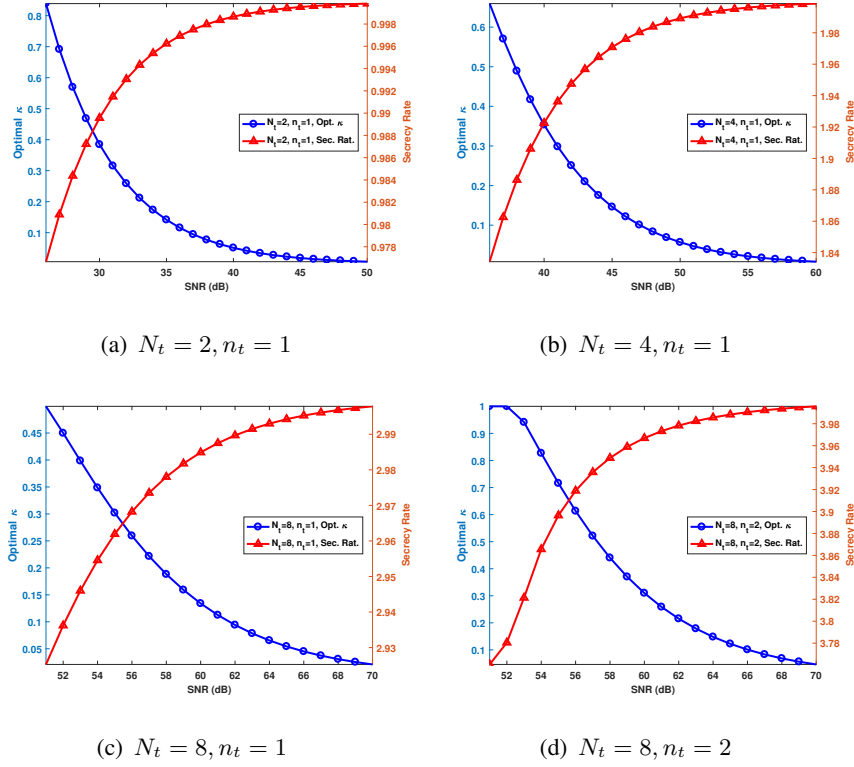


Fig. 7. Optimal power sharing factor  $\kappa$  and corresponding achievable secrecy rate versus SNR at high-SNR region. (a)  $N_t = 2, n_t = 1$ ; (b)  $N_t = 4, n_t = 1$ ; (c)  $N_t = 8, n_t = 1$ ; (d)  $N_t = 8, n_t = 2$ . The results were calculated from (37) and (38).

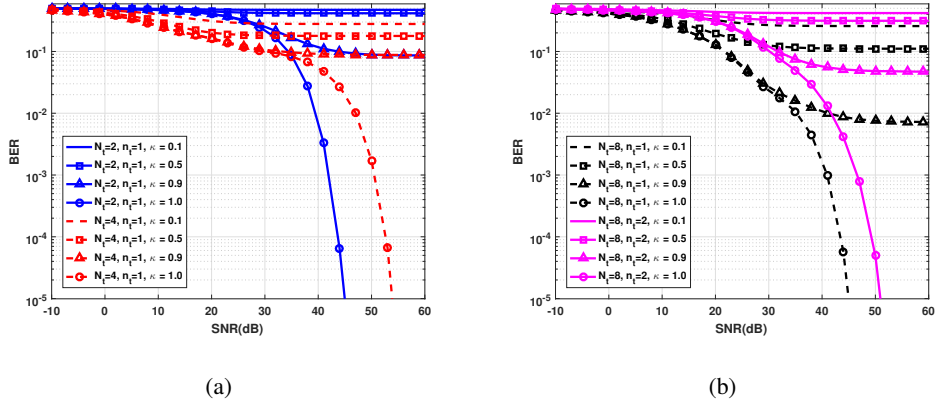


Fig. 8. BER performance of E with  $\kappa = 0.1, 0.5, 0.9$  and  $1$  for different systems, where  $N_t = 2, 4, 8$  for the SSK-VLC systems and  $N_t = 8, n_t = 2$  for our GSSK-VLC system. E is located at  $(2.60, 0.88, 0.85)$  m. (a)  $N_t = 2, 4, n_t = 1$ ; (b)  $N_t = 8, n_t = 1, 2$ . All other parameters involved in this simulation are taken from Table I and Table II.

Explicitly, Fig. 9 characterizes the impact of the power sharing factor  $\kappa$  on the BER performance of the S-D link, where we have  $N_t = 2, 4, 8$  for the SSK-VLC systems and  $N_t = 8, n_t = 2$  for the GSSK-VLC system, D is located at  $(2.15, 1.28, 0.85)$  m and we depict the BER versus SNR performance results of D by letting  $\kappa = 0.1 : 0.1 : 1$ , respectively, all other parameters involved in this simulation are taken from Table I and Table II. Using the same settings as in Fig. 9, we demonstrate the impact of the power sharing factor  $\kappa$  on the

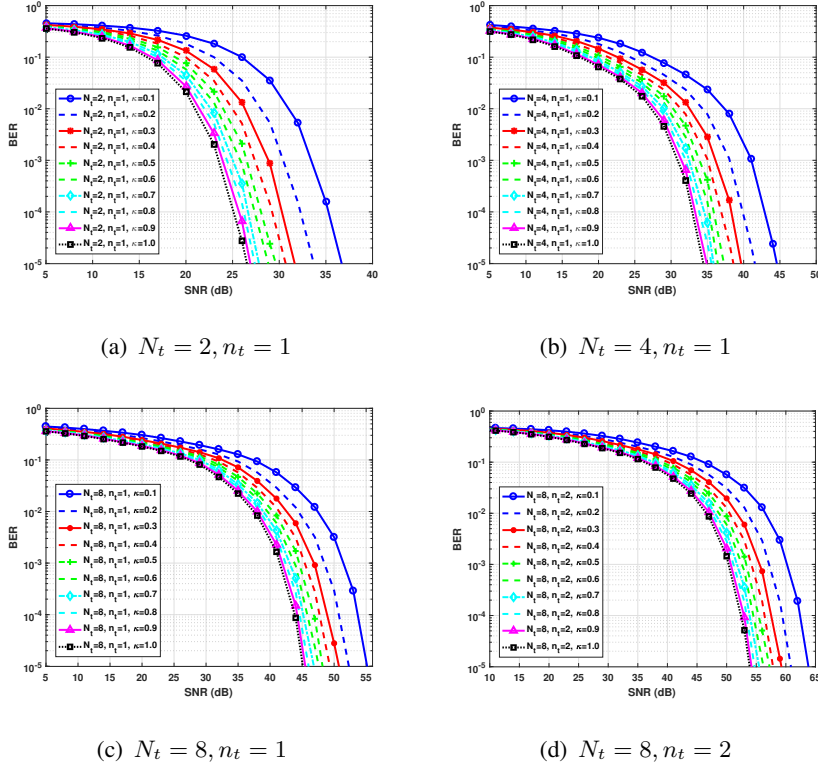


Fig. 9. BER performance of S-D link vs.  $\kappa$  of our GSSK-VLC systems. (a)  $N_t = 2, n_t = 1$ ; (b)  $N_t = 4, n_t = 1$ ; (c)  $N_t = 8, n_t = 1$ ; (d)  $N_t = 8, n_t = 2$ .

achievable secrecy rate of the systems as well, which are shown in Fig. 10. We can readily find from Fig. 9 that the BER performance of D is affected by the power sharing schemes. As shown in Fig. 9, the BER performance of D can be enhanced, when a higher percentage of power is assigned to it. However, even if more power is allocated to D, relying on  $\kappa \geq 0.5$ , the BER performance improvement of D remains modest for the GSSK-VLC systems investigated, while the achievable secrecy rate is dramatically decreased as demonstrated in Fig. 10. Hence, how to determine the optimal power sharing factor for striking a trade-off between the hypothetical by achievable secrecy rate and the desired BER performance becomes critical for practical applications.

From the results shown in Fig. 9 and 10, we can observe that for all the considered four GSSK-VLC systems operating in the high-SNR region, when  $\kappa = 1$ , we get the best BER performance, while the achievable secrecy rate approaches its minimum. By contrast, when  $\kappa = 0.1$ , the BER performance becomes the worst within the SNR range considered and the system attains the best secrecy performance. We observe furthermore that, 1) For the SSK-VLC system associated with  $N_t = 2, n_t = 1$ , when  $\kappa$  varies from 1 to 0.7, the SNR degradation at a BER of  $10^{-5}$  is about 1.3 dB, whereas the achievable secrecy rate can be increased by 1 bit/symbol; 2) For the SSK-VLC system having  $N_t = 4, n_t = 1$ , when  $\kappa$

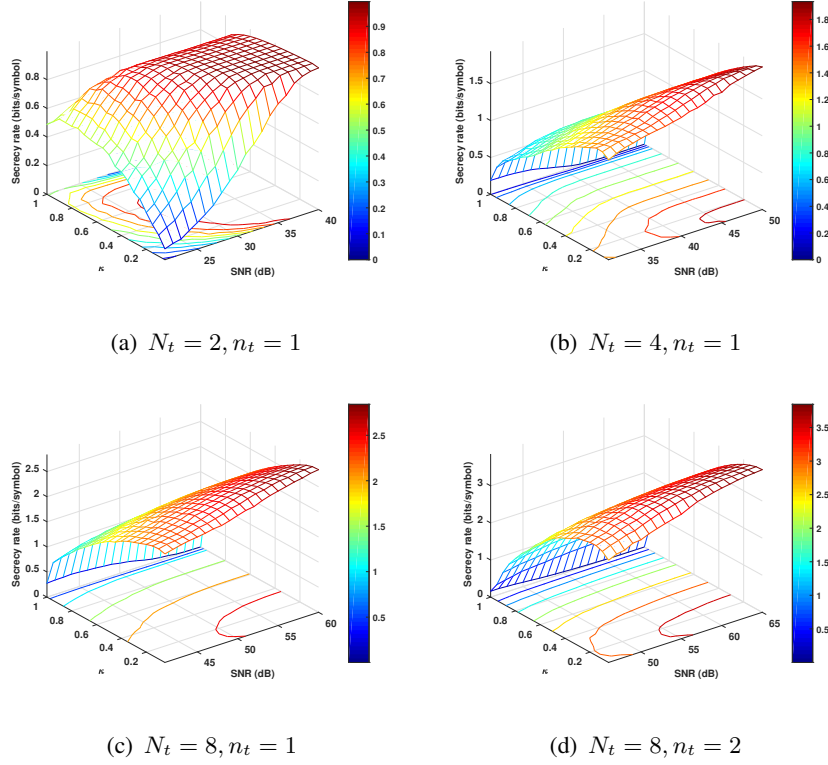


Fig. 10. Secrecy performance of the GSSK-VLC systems considered vs  $\kappa$  and SNR. (a)  $N_t = 2, n_t = 1$ ; (b)  $N_t = 4, n_t = 1$ ; (c)  $N_t = 8, n_t = 1$ ; (d)  $N_t = 8, n_t = 2$ . The results were calculated from (37) and (38).

varies from 1 to 0.5, the SNR degradation at a BER of  $10^{-5}$  is about 2.6 dB, whereas the achievable secrecy rate can be increased by 1.5 bits/symbol; 3) For the SSK-VLC system having  $N_t = 8, n_t = 1$ , when  $\kappa$  varies from 1 to 0.5, the SNR degradation at a BER of  $10^{-5}$  is about 3 dB, whereas the achievable secrecy rate can be increased by 2.5 bits/symbol; 4) For the GSSK-VLC system using  $N_t = 8, n_t = 2$ , when  $\kappa$  varies from 1 to 0.5, the SNR degradation at a BER of  $10^{-5}$  is about 3.2 dB, whereas the achievable secrecy rate can be increased by 3 bits/symbol.

From Fig. 9 and 10, we can conclude that the achievable secrecy rate increases, as more power is assigned to the jamming signals, *i.e.* for smaller  $\kappa$ . However, when a low power is allocated to the confidential information signal, the BER of the S-D link is degraded, especially when  $\kappa$  is less than 0.5. The trade-off between the secrecy performance and the BER performance should be carefully considered for each application. Based on our analysis, a look-up table can be constructed to guide the system design of the optical jamming aided GSSK-VLC systems, so that the system parameters can be optimal by selected for the system considered. If the system is secrecy-critical, we may opt for a relatively low power sharing factor  $\kappa$  based on Theorem 3 and Theorem 4. Otherwise, if the BER performance is the most important metric of the system considered, then more power should be allocated to the

information signals. For the GSSK-VLC systems jointly considering the secrecy and BER performance, based on the above results, we can opt for a power sharing factor of  $\kappa = 0.5$  in the relatively high-SNR region and  $\kappa = 1$  in the lower-SNR region.

## VI. CONCLUSIONS

As a recent secrecy enhancement strategy, PLS has been shown to be unbreakable, regardless of the computational capability of E. Given the broadcast nature of the VLC downlink, it is advisable to improve its secrecy. In this paper, we have provided the secrecy performance analysis of a PLS-aided GSSK-VLC system. Accordingly, four major contributions have been proposed. Firstly, by exploiting the input signal characteristics and channels of the proposed GSSK-VLC system, the secrecy performance was analyzed, when the input signals are assumed to have finite discrete distributions subject to specific amplitude and power constraints. From these results, we conclude that without extra secrecy enhancement, E may wiretap the confidential signals at high SNRs, even if its channel conditions are worse than those of D. Moreover, if the S-D channel is degraded, the system fails to support secret communication. Secondly, a friendly optical jamming aided secrecy enhancement scheme was designed for the proposed GSSK-VLC system. Apart from transmitting optical jamming signals by the LEDs, S sends simultaneously its confidential signal using these LEDs under appropriate amplitude and power constraints. We adopted the truncated Gaussian distribution for the optical jamming signals to satisfy these constraints. Furthermore, the optical jamming signals were generated within the nullspace of the S-D channel vector. Thirdly, the secrecy performance of our GSSK-VLC system relying on optical jamming was analyzed. Fourthly, the optimal power sharing strategy of the proposed GSSK-VLC system using optical jamming was considered for maximizing the achievable secrecy rate of the proposed system. Specifically, the closed-form expressions of the optimal power sharing were derived both for the low- and high-SNR regions. Finally, all the analytical results have been verified by computer simulations. Additionally, a power sharing factor selection technique has been proposed for striking a trade-off between the secrecy and BER performance.



## APPENDIX

## A. Proof of Theorem 1

Based on (20)-(23), the AMI  $\mathbb{I}^J(h_D; Y)$  can be expressed as

$$\begin{aligned} \mathbb{I}^J(h_D; Y) &= \sum_{\omega=1}^M \int_y f_{Y, h_D}(h = h_{D(\omega)}, y) \log_2 \frac{f_{Y|h_D}(y|h_D = h_{D(\omega)})}{p_Y(y)} dy \\ &= \log_2 M - \frac{1}{M} \sum_{\omega=1}^M \mathbb{E}_{w_D} \left[ \log_2 \sum_{\varpi=1}^M \exp \left( \frac{w_D^2 - (w_D + (h_{D(\omega)} - h_{D(\varpi)})s)^2}{2\sigma_D^2} \right) \right]. \end{aligned} \quad (39)$$

Using the notation  $\zeta_{\omega, \varpi} = h_{D(\omega)} - h_{D(\varpi)}$ , (39) can be expressed as

$$\mathbb{I}(h_D; Y) = \log_2 M - \frac{1}{M} \sum_{\omega=1}^M \mathbb{E}_{w_D} \left[ \log_2 \sum_{\varpi=1}^M \exp \left( \frac{1}{2} \varrho_D (w_D^2 - (w_D + \zeta_{\omega, \varpi} s)^2) \right) \right], \quad (40)$$

where  $\varrho_D = 1/\sigma_D^2$ . It can be shown that for a particular  $\zeta_{\omega, \varpi}$  and  $s$ ,  $\mathbb{I}(h_D; Y)$  is a monotonically increasing function w.r.t. the SNR  $\varrho_D$ . For  $\varrho_D \rightarrow \infty$ , i.e.,  $\sigma_D^2 = 0$ , we have

$$\lim_{\varrho_D \rightarrow \infty} \mathbb{I}(h_D; Y) = \log_2 M, \quad (41)$$

which is the upper bound of  $\mathbb{I}(h_D; Y)$ .

In a similar way, when using the notation of  $\xi_{\omega, \varpi} = h_{E(\omega)} - h_{E(\varpi)}$ , the AMI of the S-E channel can be expressed as

$$\mathbb{I}^J(\mathbf{h}_E; Z) = \log_2 M - \frac{1}{M} \sum_{\omega=1}^M \mathbb{E}_{\tilde{w}_E} \left[ \log_2 \sum_{\varpi=1}^M \exp \left( \frac{1}{2} \left( \tilde{w}_E^2 - (\tilde{w}_E + \Omega_E^{-1/2} \xi_{\omega, \varpi} s)^2 \right) \right) \right]. \quad (42)$$

## B. Proof of Theorem 2

The proof of (26) and that of (27) are the same. Therefore, in the following, we only detail the proof of (27).

From (25), we have

$$\begin{aligned} \mathbb{I}^J(h_E; Z) &= \log_2 M - \frac{1}{M} \sum_{\omega=1}^M \mathbb{E}_{\tilde{w}_E} \left[ \log_2 \exp \left( \frac{\tilde{w}_E^2}{2} \right) \right] \\ &\quad - \frac{1}{M} \sum_{\omega=1}^M \mathbb{E}_{\tilde{w}_E} \left[ \log_2 \sum_{\varpi=1}^M \exp \left( - \frac{(\tilde{w}_E + \Omega_E^{-1/2} \xi_{\omega, \varpi} s)^2}{2} \right) \right] \\ &= \log_2 M - I_1^J - I_2^J. \end{aligned} \quad (43)$$

The second term at the RHS of (43), i.e.,  $I_1^J$ , can be simplified as

$$I_1^J = \frac{1}{M} \sum_{\omega=1}^M \mathbb{E}_{\tilde{w}_E} \left[ \log_2 \exp \left( \frac{\tilde{w}_E^2}{2} \right) \right] = \log_2 e \mathbb{E}_{\tilde{w}_E} \left[ \frac{\tilde{w}_E^2}{2} \right] = \frac{1}{2} \log_2 e. \quad (44)$$

Due to the concavity of  $\log_2(\cdot)$ , the third term at the RHS of (43), i.e.,  $I_2^J$ , can be upper bounded by applying Jensen's inequality as

$$\begin{aligned} I_2^J &\leq \frac{1}{M} \sum_{\omega=1}^M \log_2 \sum_{\varpi=1}^M \mathbb{E}_{\tilde{w}_E} \left[ \exp \left( -\frac{\left( \tilde{w}_E + \Omega_E^{-1/2} \xi_{\omega, \varpi} s \right)^2}{2} \right) \right] \\ &= -\frac{1}{2} + \frac{1}{M} \sum_{\omega=1}^M \log_2 \sum_{\varpi=1}^M \exp \left( -\frac{(\xi_{\omega, \varpi} s)^2}{4\Omega_E} \right). \end{aligned} \quad (45)$$

Finally, upon substituting (44) and (45) into (43), we can arrive at:

$$\mathbb{I}^J(h_E; Z) \geq \log_2 M - \frac{1}{2}(\log_2 e - 1) - \frac{1}{M} \sum_{\omega=1}^M \log_2 \sum_{\varpi=1}^M \exp \left( -\frac{(\xi_{\omega, \varpi} s)^2}{4\Omega_E} \right), \quad (46)$$

which completes the proof of Theorem 2.

### C. Proof of Theorem 3

Let us first consider the situation, where the SNR is very low, that is  $\rho \ll 1$ . Then, from (30), we have

$$\begin{aligned} \Upsilon_1 &= \sum_{\omega=1}^M \log_2 \sum_{\varpi=1}^M \exp \left( -\frac{(\xi_{\omega, \varpi} s)^2}{4\sigma^2} \right) \stackrel{(a)}{\approx} \sum_{\omega=1}^M \log_2 \sum_{\varpi=1}^M \left( 1 - \frac{\rho \kappa \mathcal{P} \xi_{\omega, \varpi}^2}{4} \right) \\ &\stackrel{(b)}{\approx} M \log_2 M + \log_2 \left( 1 - \frac{\rho \kappa \mathcal{P}}{4} \sum_{\omega=1}^M d_{\omega} \right) = M \log_2 M + \log_2 \left( 1 - \frac{1}{4} \rho \kappa \mathcal{P} M \bar{d} \right), \end{aligned} \quad (47)$$

where we have (a) by applying the approximation by the Taylor series. For small  $\rho$ , we have (b) by letting  $\rho \rightarrow 0$ .

Similarly, from (31), we have

$$\begin{aligned} \Upsilon_2 &= \sum_{\omega=1}^M \log_2 \sum_{\varpi=1}^M \exp \left( -\frac{(\xi_{\omega, \varpi} s)^2}{4\Omega_E} \right) = \sum_{\omega=1}^M \log_2 \sum_{\varpi=1}^M \exp \left( -\frac{\xi_{\omega, \varpi}^2 \kappa \mathcal{P}}{4(\chi \sigma_u^2 + \sigma^2)} \right) \\ &= \sum_{\omega=1}^M \log_2 \sum_{\varpi=1}^M \exp \left( -\frac{\rho \kappa \mathcal{P} \xi_{\omega, \varpi}^2}{4(\rho(1-\kappa)\mathcal{P}\chi + 1)} \right) \stackrel{(a)}{\approx} \sum_{\omega=1}^M \log_2 \sum_{\varpi=1}^M \exp \left( -\frac{\rho \kappa \mathcal{P} \xi_{\omega, \varpi}^2}{4} \right) \\ &\stackrel{(b)}{\approx} \sum_{\omega=1}^M \log_2 \sum_{\varpi=1}^M \left( 1 - \frac{\rho \kappa \mathcal{P} \xi_{\omega, \varpi}^2}{4} \right) = \sum_{\omega=1}^M \log_2 \left( M \left( 1 - \frac{\rho \kappa \mathcal{P} g_{\omega}}{4} \right) \right) \\ &\stackrel{(c)}{\approx} M \log_2 M + \log_2 \left( 1 - \frac{\rho \kappa \mathcal{P}}{4} \sum_{\omega=1}^M g_{\omega} \right) = M \log_2 M + \log_2 \left( 1 - \frac{1}{4} \rho \kappa \mathcal{P} M \bar{g} \right), \end{aligned} \quad (48)$$

where again, we have (a) and (c) due to  $\varrho \ll 1$  and we have (b) by the Taylor expansion and approximation. By substituting (47) and (48) into (32), we obtain

$$R_{S,\text{sec}}^J(\kappa) = \mathbb{I}_S^J(h_D; Y) - \mathbb{I}_S^J(h_E; Z) = \frac{1}{M}(\Upsilon_2 - \Upsilon_1) \quad (49)$$

$$= \frac{1}{M} \log_2 \frac{1 - \frac{1}{4}\varrho\mathcal{P}M\bar{g}\kappa}{1 - \frac{1}{4}\varrho\mathcal{P}M\bar{d}\kappa}. \quad (50)$$

We can readily verify that when  $\bar{d} > \bar{g}$ ,  $R_{S,\text{sec}}^J(\kappa)$  is a monotonically increasing function of  $\kappa \in [0, 1]$ . By contrast, when  $\bar{d} < \bar{g}$ ,  $R_{S,\text{sec}}^J(\kappa)$  is a monotonically decreasing function of  $\kappa \in [0, 1]$ . Therefore, when operated in the low-SNR region, and when  $\bar{d} > \bar{g}$ ,  $R_{S,\text{sec}}^J(\kappa)$  attains its maximum at  $\kappa = 1$ . When  $\bar{d} < \bar{g}$ ,  $R_{S,\text{sec}}^J(\kappa)$  achieves its maximum at  $\kappa = 0$ , implying that we should allocate as much power as possible to the jamming signals. It should be noted that the achievable secrecy rate  $R_{S,\text{sec}}^J(\kappa)$  is zero, when  $\bar{d} < \bar{g}$  and  $\varrho \ll 1$ <sup>1</sup>.

#### D. Proof of Theorem 4

Let us now consider the situation of the high-SNR region with  $\varrho \gg 1$ . Due to value ranges of  $\varrho, \kappa$ , one of the following three cases should be satisfied by the product of  $\varrho\kappa$ , which are 1)  $\varrho\kappa \rightarrow 0$ ; 2)  $\varrho\kappa = c_1$ , where  $c_1$  is a finite real-valued constant; 3)  $\varrho\kappa \rightarrow \infty$ .

In the first case, (32) is used for calculating  $R_{S,\text{sec}}^J(\kappa)$ , which implies that  $\kappa \rightarrow 0$  and gives  $R_{S,\text{sec}}^J(\kappa) = 0$ . Hence, there exist no values of  $\kappa \in (0, 1)$  that are optimal. In the second case,  $\varrho \rightarrow \infty$  also results in  $\kappa \rightarrow 0$ , hence we have  $R_{S,\text{sec}}^J(\kappa) = 0$ . In the third case, when  $\varrho\kappa \rightarrow \infty$ , we can infer from (32) that  $R_{S,\text{sec}}^J(\kappa) \approx \frac{1}{M} \sum_{\omega=1}^M \log_2 \sum_{\varpi=1}^M \exp\left(-\frac{\kappa\mathcal{P}\xi_{\omega,\varpi}^2}{4(1-\kappa)\mathcal{P}\chi}\right) + c$ , where  $c$  is a constant. Explicitly, the highest  $R_{S,\text{sec}}^J(\kappa)$  is obtained with an optimal  $\kappa$  approaching 0. From the analysis of the above three cases, we can conclude that the optimal value of  $\kappa$  is close to zero, when operating in the high-SNR region. In other words, in the high-SNR region, the optimal  $\kappa$  should be a relative small value. Based on these observations, we define the optimal  $\kappa$  in the high-SNR region as follows.

We commence by considering  $\Upsilon_1$  in the high-SNR region, which can be approximated as

$$\begin{aligned} \Upsilon_1 &= \sum_{\omega=1}^M \log_2 \sum_{\varpi=1}^M \exp\left(-\frac{(\zeta_{\omega,\varpi} s)^2}{4\sigma^2}\right) = \sum_{\omega=1}^M \log_2 \sum_{\varpi=1}^M \exp\left(-\frac{\varrho\kappa\mathcal{P}\zeta_{\omega,\varpi}^2}{4}\right) \\ &= \sum_{\omega=1}^M \log_2 \left[1 + \sum_{\varpi=1, \varpi \neq \omega}^M \exp\left(-\frac{\varrho\kappa\mathcal{P}\zeta_{\omega,\varpi}^2}{4}\right)\right]. \end{aligned} \quad (51)$$

<sup>1</sup>In practical systems, we should use the resource-allocation to ensure that  $\bar{d} > \bar{g}$ .

Since  $\exp(-\delta)$  is a rapidly decaying function w.r.t. a positive  $\delta$ , we can introduce the approximation of

$$\sum_{\varpi=1, \varpi \neq \omega}^{N_t} \exp\left(-\frac{\varrho \kappa \mathcal{P} \zeta_{\omega, \varpi}^2}{4}\right) \approx \ell_{\omega} \exp\left(-\frac{\varrho \kappa \mathcal{P} \zeta_{\omega}^{\min}}{4}\right). \quad (52)$$

Then,  $\Upsilon_1$  can be approximated as

$$\begin{aligned} \Upsilon_1 &\approx \sum_{\omega=1}^M \log_2 \left[ 1 + \ell_{\omega} \exp\left(-\frac{\varrho \kappa \mathcal{P} \zeta_{\omega}^{\min}}{4}\right) \right] = \log_2 \prod_{\omega=1}^M \left[ 1 + \ell_{\omega} \exp\left(-\frac{\varrho \kappa \mathcal{P} \zeta_{\omega}^{\min}}{4}\right) \right] \\ &\stackrel{(a)}{\approx} \log_2 \left[ 1 + \sum_{\omega=1}^M \ell_{\omega} \exp\left(-\frac{\varrho \kappa \mathcal{P} \zeta_{\omega}^{\min}}{4}\right) \right] \stackrel{(b)}{\approx} \log_2 \left[ 1 + \ell \exp\left(-\frac{\varrho \kappa \mathcal{P} \zeta^{\min}}{4}\right) \right], \end{aligned} \quad (53)$$

where both (a) and (b) hold due to the fact that  $\kappa$  is a small real number approaching 0.

The term  $\Upsilon_2$  defined under (32) in the high-SNR region can be approximated as

$$\begin{aligned} \Upsilon_2 &= \sum_{\omega=1}^M \log_2 \sum_{\varpi=1}^M \exp\left(-\frac{(\xi_{\omega, \varpi} s)^2}{4\Omega_E}\right) = \sum_{\omega=1}^M \log_2 \sum_{\varpi=1}^M \exp\left(-\frac{\varrho \kappa \mathcal{P} \xi_{\omega, \varpi}^2}{4(\varrho(1-\kappa)\mathcal{P}\chi + 1)}\right) \\ &\stackrel{(a)}{\approx} \sum_{\omega=1}^M \log_2 \sum_{\varpi=1}^M \exp\left(-\frac{\kappa \xi_{\omega, \varpi}^2}{4(1-\kappa)\chi}\right) \stackrel{(b)}{\approx} \sum_{\omega=1}^M \log_2 \sum_{\varpi=1}^M \exp\left(-\frac{\kappa \xi_{\omega, \varpi}^2}{4\chi}\right) \\ &\stackrel{(c)}{\approx} \sum_{\omega=1}^M \log_2 \sum_{\varpi=1}^M \left(1 - \frac{\kappa \xi_{\omega, \varpi}^2}{4\chi}\right) = \sum_{\omega=1}^M \log_2 \left(M \left(1 - \frac{\kappa g_{\omega}}{4\chi}\right)\right) \\ &\approx M \log_2 M + \log_2 \left(1 - \frac{\kappa}{4\chi} \sum_{\omega=1}^M g_{\omega}\right) = M \log_2 M + \log_2 \left(1 - \frac{1}{4\chi} \kappa M \bar{g}\right), \end{aligned} \quad (54)$$

where we have (a) due to  $\varrho \rightarrow \infty$ ; we have (b) owing to  $\kappa \rightarrow 0$ ; (c) follows according to the Taylor approximation.

Upon substituting (53) and (54) into (32), we obtain

$$\begin{aligned} R_{S, \text{sec}}^J(\kappa) &= \frac{1}{M} (\Upsilon_2 - \Upsilon_1) \\ &= \log_2 M + \frac{1}{M} \left[ \log_2 \left(1 - \frac{1}{4\chi} \kappa M \bar{g}\right) - \log_2 \left[ 1 + \ell \exp\left(-\frac{\varrho \kappa \mathcal{P} \zeta^{\min}}{4}\right) \right] \right]. \end{aligned} \quad (55)$$

Since  $\log_2 \left(1 - \frac{1}{4\chi} \kappa M \bar{g}\right)$  is a log-concave function and  $1 + \ell \exp\left(-\frac{\varrho \kappa \mathcal{P} \zeta^{\min}}{4}\right)$  is a log-convex function both w.r.t.  $\kappa$ ,  $R_{S, \text{sec}}^J(\kappa)$  is a concave function of  $\kappa$ . Therefore, the maximum of  $R_{S, \text{sec}}^J(\kappa)$  is achieved, when  $\kappa$  satisfies

$$\frac{\partial R_{S, \text{sec}}^J(\kappa)}{\partial \kappa} = \frac{1}{M} \left[ \frac{-\frac{1}{4\chi} M \bar{g}}{1 - \frac{\kappa M \bar{g}}{4\chi}} - \frac{\ell \exp\left(-\frac{\varrho \kappa \mathcal{P} \zeta^{\min}}{4}\right) \left(-\frac{\varrho \mathcal{P} \zeta^{\min}}{4}\right)}{1 + \ell \exp\left(-\frac{\varrho \kappa \mathcal{P} \zeta^{\min}}{4}\right)} \right] = 0. \quad (56)$$

Explicitly, we have  $1 - \frac{\kappa M \bar{g}}{4\chi} \xrightarrow{\kappa \rightarrow 0} 1$ . With the aid of this approximation, the desired result in (37) can be obtained by the solution of (56).

## REFERENCES

- [1] L. Hanzo, H. Haas, S. Imre, D. O'Brien, M. Rupp, and L. Gyongyosi, "Wireless myths, realities, and futures: From 3G/4G to optical and quantum wireless," *Proc. IEEE*, vol. 100, no. Special Centennial Issue, pp. 1853–1888, May 2012.
- [2] H. Elgala, R. Mesleh, and H. Haas, "Indoor optical wireless communication: Potential and state-of-the-art," *IEEE Commun. Mag.*, vol. 49, no. 9, pp. 56–62, Sep. 2011.
- [3] D. Karunatilaka, F. Zafar, V. Kalavally, and R. Parthiban, "LED based indoor visible light communications: State of the art," *IEEE Commun. Surveys Tuts.*, vol. 17, no. 3, pp. 1649–1678, 2015.
- [4] R. Zhang, H. Claussen, H. Haas, and L. Hanzo, "Energy efficient visible light communications relying on amorphous cells," *IEEE J. Sel. Areas Commun.*, vol. 34, no. 4, pp. 894–906, Apr. 2016.
- [5] A. Mostafa and L. Lampe, "Physical-Layer security for MISO visible light communication channels," *IEEE J. Sel. Areas Commun.*, vol. 33, no. 9, pp. 1806–1818, Sep. 2015.
- [6] J. Classen, J. Chen, D. Steinmetzer, M. Hollick, and E. Knightly, "The spy next door: Eavesdropping on high throughput visible light communications," in *Proc. ACM VLCS'2015*, Paris, Sep. 2015, pp. 9–14.
- [7] J. Classen, D. Steinmetzer, and M. Hollick, "Opportunities and pitfalls in securing visible light communication on the physical layer," in *Proc. ACM VLCS'2016*, New York, Oct. 2016, pp. 19–24.
- [8] Y. S. Shiu, S. Y. Chang, H. C. Wu, S. C. H. Huang, and H. H. Chen, "Physical layer security in wireless networks: A tutorial," *IEEE Wireless Commun.*, vol. 18, no. 2, pp. 66–74, Apr. 2011.
- [9] Y.-W. P. Hong, P.-C. Lan, and C.-C. J. Kuo, *Signal Processing Approaches to Secure Physical Layer Communications in Multi-Antenna Wireless Systems*. New York, NY, USA: Springer-Verlag, 2014.
- [10] Y. Zou, J. Zhu, X. Wang, and L. Hanzo, "A survey on wireless security: Technical challenges, recent advances, and future trends," *Proc. IEEE*, vol. 104, no. 9, pp. 1727–1765, Sep. 2016.
- [11] X. Chen, D. W. K. Ng, W. Gerstacker, and H. H. Chen, "A survey on multiple-antenna techniques for physical layer security," *IEEE Commun. Surveys Tuts.*, vol. 19, no. 2, pp. 1027–1053, 2016.
- [12] Y. Liu, H. H. Chen, and L. Wang, "Physical layer security for next generation wireless networks: Theories, technologies, and challenges," *IEEE Commun. Surveys Tuts.*, vol. 19, no. 1, pp. 347–376, 2017.
- [13] S. R. Aghdam and T. M. Duman, "Joint precoder and artificial noise design for MIMO wiretap channels with finite-alphabet inputs based on the cut-off rate," *IEEE Trans. Wireless Commun.*, vol. 16, no. 6, pp. 3913–3923, Jun. 2017.
- [14] A. D. Wyner, "The wire-tap channel," *Bell Syst. Tech. J.*, vol. 54, no. 8, pp. 1355–1387, Oct. 1975.
- [15] I. Csiszar and J. Korner, "Broadcast channels with confidential messages," *IEEE Trans. Inf. Theory*, vol. 24, no. 3, pp. 339–348, May 1978.
- [16] S. Leung-Yan-Cheong and M. Hellman, "The Gaussian wire-tap channel," *IEEE Trans. Inf. Theory*, vol. 24, no. 4, pp. 451–456, Jul. 1978.
- [17] A. Lapidoto, S. M. Moser, and M. A. Wigger, "On the capacity of free-space optical intensity channels," *IEEE Trans. Inf. Theory*, vol. 55, no. 10, pp. 4449–4461, Oct. 2009.
- [18] A. Chaaban, J. M. Morvan, and M. S. Alouini, "Free-space optical communications: Capacity bounds, approximations, and a new sphere-packing perspective," *IEEE Trans. Commun.*, vol. 64, no. 3, pp. 1176–1191, Mar. 2016.
- [19] R. Jiang, Z. Wang, Q. Wang, and L. Dai, "A tight upper bound on channel capacity for visible light communications," *IEEE Commun. Lett.*, vol. 20, no. 1, pp. 97–100, Jan. 2016.
- [20] A. Chaaban, Z. Rezk, and M. S. Alouini, "Fundamental limits of parallel optical wireless channels: Capacity results and outage formulation," *IEEE Trans. Commun.*, vol. 65, no. 1, pp. 296–311, Jan. 2017.

- [21] A. Mostafa and L. Lampe, "Securing visible light communications via friendly jamming," in *Proc. IEEE GLOBECOM Wkshps'2014*, Dec. 2014, pp. 524–529.
- [22] H. Zaid, Z. Rezki, A. Chaaban, and M. S. Alouini, "Improved achievable secrecy rate of visible light communication with cooperative jamming," in *Proc. IEEE GLOBALSIP'2015*, Dec. 2015, pp. 1165–1169.
- [23] S. Ma, Z. L. Dong, H. Li, Z. Lu, and S. Li, "Optimal and robust secure beamformer for indoor MISO visible light communication," *J. Lightw. Technol.*, vol. 34, no. 21, pp. 4988–4998, Nov. 2016.
- [24] A. Mostafa and L. Lampe, "Optimal and robust beamforming for secure transmission in MISO visible-light communication links," *IEEE Trans. Signal Process.*, vol. 64, no. 24, pp. 6501–6516, Dec. 2016.
- [25] S. Goel and R. Negi, "Guaranteeing secrecy using artificial noise," *IEEE Trans. Wireless Commun.*, vol. 7, no. 6, pp. 2180–2189, Jun. 2008.
- [26] H. Shen, Y. Deng, W. Xu, and C. Zhao, "Secrecy-oriented transmitter optimization for visible light communication systems," *IEEE Photo. J.*, vol. 8, no. 5, pp. 1–14, Oct. 2016.
- [27] M. A. Arfaoui, Z. Rezki, A. Ghayeb, and M. S. Alouini, "On the secrecy capacity of MISO visible light communication channels," in *Proc. IEEE GLOBECOM'2016*, Dec. 2016, pp. 1–7.
- [28] O. Ozel, E. Ekrem, and S. Ulukus, "Gaussian wiretap channel with amplitude and variance constraints," *IEEE Trans. Inf. Theory*, vol. 61, no. 10, pp. 5553–5563, Oct. 2015.
- [29] H. Qin, Y. Sun, T. H. Chang, X. Chen, C. Y. Chi, M. Zhao, and J. Wang, "Power allocation and time-domain artificial noise design for wiretap OFDM with discrete inputs," *IEEE Trans. Wireless Commun.*, vol. 12, no. 6, pp. 2717–2729, Jun. 2013.
- [30] Y. Liang, H. V. Poor, and S. Shamai, "Secure communication over fading channels," *IEEE Trans. Inf. Theory*, vol. 54, no. 6, pp. 2470–2492, Jun. 2008.
- [31] R. Mesleh, H. Elgala, and H. Haas, "Optical spatial modulation," *IEEE/OSA J. Optical Commun. Netw.*, vol. 3, no. 3, pp. 234–244, Mar. 2011.
- [32] T. Fath and H. Haas, "Performance comparison of MIMO techniques for optical wireless communications in indoor environments," *IEEE Trans. Commun.*, vol. 61, no. 2, pp. 733–742, Feb. 2013.
- [33] W. O. Popoola, E. Poves, and H. Haas, "Error performance of generalised space shift keying for indoor visible light communications," *IEEE Trans. Commun.*, vol. 61, no. 5, pp. 1968–1976, May 2013.
- [34] A. Stavridis and H. Haas, "Performance evaluation of space modulation techniques in VLC systems," in *Proc. IEEE ICC'2015*, Jun. 2015, pp. 1356–1361.
- [35] L. Zeng, D. C. O'Brien, H. L. Minh, G. E. Faulkner, K. Lee, D. Jung, Y. Oh, and E. T. Won, "High data rate multiple input multiple output (MIMO) optical wireless communications using white LED lighting," *IEEE J. Sel. Areas Commun.*, vol. 27, no. 9, pp. 1654–1662, Dec. 2009.
- [36] J. M. Kahn and J. R. Barry, "Wireless infrared communications," *Proc. IEEE*, vol. 85, no. 2, pp. 265–298, Feb. 1997.
- [37] R. A. Horn and C. R. Johnson, *Matrix Analysis*, 2nd ed. New York, NY, USA: Cambridge University Press, 2012.
- [38] Z. I. Botev, "The normal law under linear restrictions: Simulation and estimation via minimax tilting," *J. Royal Stat. Soc.: Ser. B-Stat. Methodol.*, vol. 79, no. 1, pp. 125–148, Jan. 2017.
- [39] R. G. Gallager, *Information theory and reliable communication*. Hoboken, NJ, USA: Wiley, 1968.
- [40] F. Wang, C. Liu, Q. Wang, J. Zhang, R. Zhang, L.-L. Yang, and L. Hanzo, "Secrecy performance analysis of visible light communication systems with generalized space-shift keying modulation," *Submitted for publication*, 2017.
- [41] X. Li, F. Jin, R. Zhang, J. Wang, Z. Xu, and L. Hanzo, "Users first: User-centric cluster formation for interference-mitigation in visible-light networks," *IEEE Trans. Wireless Commun.*, vol. 15, no. 1, pp. 39–53, Jan. 2016.